Università degli Studi di Padova

Dipartimento di Ingegneria Industriale DII

Corso di Laurea Magistrale in Ingegneria Aerospaziale

Analytical preliminary investigation for an experimental radial mode analysis in a multi-stage axial compressor test rig

Relatore: Prof. Ernesto Benini
Correlatore: Dr.-Ing. Herwart Hönen

Studente: Giorgia Tescaro
Matricola: 1153681

Anno Accademico 2018/2019

Contents

List of Figures

List of Tables

List of symbols

Symbol	Meaning	Unit
$\mathbf{a}$	Vector of radial mode amplitudes	Pa
A_m	Azimuthal mode amplitudes	Pa
$A_{mn}^{\pm}$	Radial mode complex amplitudes	Pa
B	Number of rotor's blades	[-]
c	Sound velocity	$m \cdot s^{-1}$
f_{mn}	Radial shape factor	[-]
f_{BPF}	Blade Passing Frequency	s^{-1}
f_R	Rotor turn frequency	s^{-1}
h	Blade Passing Frequency harmonic	[-]
k	Wave number in free-field conditions	[-]
$k_{mn}^{\pm}$	Axial wave number of the mode	m^{-1}
m	Number of azimuthal mode order	[-]
M_x	Flow axial Mach number	[-]
M_Φ	Circumferential Mach number	[-]
n	Number of radial mode order	[-]
N	Rotor shaft speed	s^{-1}
N_r	Number of radial measuring locations	[-]
N_x	Number of axial measuring planes	[-]
N_Φ	Number of azimuthal measuring points	[-]
p	Acoustic complex pressure	Pa
$\mathbf{p}$	Vector of the measured acoustic pressure	Pa
Q_{mn}	Eigenvalue of the mode	[-]
r	Radial coordinate	m
R	Outer duct radius	m
R_i	Inner duct radius	m
$\mathbf{U}$	Vector of the stationary flow speed	$m \cdot s^{-1}$
V	Number of stator vanes	[-]
$\mathbf{W}$	Matrix of the radial mode analysis	[-]
x	Axial coordinate	m
δA	Relative error	[-]
η	Hub-to-tip ratio	[-]
κ	Condition number of matrix $\mathbf{W}$	[-]
Φ	Azimuthal coordinate	rad
ω	Rotor shaft angular speed	$rad \cdot s^{-1}$
Ω_m	Spin rate of the mode	$rad \cdot s^{-1}$
Ω_s	Angular velocity of the component of the flow swirl	$rad \cdot s^{-1}$
ϱ	Density	$kg \cdot m^{-3}$
σ_{mn}	Eigenvalue of the mode	[-]
θ	Flow angle in an absolute coordinate system	rad

Abstract

La generazione e la propagazione del suono all'interno di una turbomacchina sono oggetto di studio per migliorare e convalidare le previsioni sulla risposta forzata della struttura calcolate dai solutori CFD.
Tramite simulazioni sperimentali condotte alla RWTH Aachen University è stato infatti trovato che l'acustica incide sulla risposta forzata della struttura e che differenti distribuzioni radiali di pressione possono cambiare l'eccitazione delle pale.
In questo elaborato viene presentato un metodo che permette di svolgere un'ottimizzazione di una griglia di sensori per misurazioni acustiche all'interno di un compressore assiale multi-stadio e che studia l'influenza data da errori di misura. Il metodo si basa su un'analisi modale radiale (dall'inglese Radial Mode Analysis), che permette di trovare l'ampiezza e la fase dei cosiddetti modi acustici, partendo da misurazioni sperimentali della pressione acustica all'interno del condotto. L'ottimizzazione deve essere compiuta osservando per quali parametri della griglia la qualità dell'analisi modale radiale risulta buona.
Dal processo implementato e dai risultati ottenuti si trova che l'ottimizzazione deve essere svolta studiando singolarmente ciascun modo acustico perchè i parametri ottimizzati riguardanti la griglia cambiano a seconda dei modi acustici considerati.

1. Introduction

The main purpose of this work concerns the optimization of a sensors grid for acoustic measurements in a turbomachine.
During simulations and tests carried out at the test rigs located at RWTH Aachen University, it came out that acoustics has an impact on structure's forced response. Particularly, it has been found that different radial pressure distributions can change the excitation of the blades. Hence, a detailed knowledge on the generation and propagation of sound into the duct and its effects needs to validate and compare the forced response predictions done by a CFD solver.
In contrast to acoustics in a free field, the solution of the acoustic wave equation in ducts is given by the superposition of acoustic spinning modes, which determine a singular and periodic pressure pattern. In order to know which of these modes occur in the duct and which amplitude each mode has, a Radial Mode Analysis (RMA) has to be implemented. Particularly, this analysis has in input experimental measurements of the acoustic pressure along the duct. Because the analysis quality depends on the arrangement of the measuring array, an optimization of the grid parameters is needed in order to decrease errors in the solution and, hence, to improve the prediction on forced response. Particularly, this analysis provides better validation data than the data resulting from only an Azimuthal Mode Analysis (AMA).
The turbomachine to which this work refers is a multi-stage axial compressor and the section in which the analysis is carried out is the inlet.

1.1. Set-up of the work

The present work starts with Chapter 2 illustrating briefly the theoretical principles about the generation and propagation of acoustic modes in a turbomachine. Also the analytical methods that can be implemented in order to decompose the acoustic pressure field into these modes are reported and explained.
In Chapter 3 an overview on the development of this area of studies through the years is presented, showing only some of the main works carried out in the past decades.
The implemented process of the analysis is explained in Chapter 4. The purpose of this process is to find an optimization of the measuring grid for which the accuracy of mode decomposition is maximized whereas the propagation of measuring inaccuracies due to the noise is minimized. The encountered issues during the set-up of this process are discussed.
In Chapter 5 the results coming from the analysis are displayed and a discussion com-

paring different cases and modes is carried out. Looking on these results, the parameters concerning the arrangement of the measuring grid are optimized.

2. Theoretical background

The pressure field in a duct or in ducted sections of compressors, turbines or ducted fans that are located before and after the blading sections, can present various shapes due to the multitude of sources that generate it. In 1962 Tyler and Sofrin published a study on axial flow compressor noise and demonstrated that the radiation of sound from the end of the duct depends mostly on the generation and propagation of spinning modes, which are rotating pressure patterns that present a singular and periodic shape [12][2][5].
Mathematically the pressure field can be obtained by the superposition of these modes whose shape present m periods in the circumferential direction and n nodes (the points in which the value of the function becomes zero) in the radial direction for every axial plane in the duct. Hence, it is said that the mode has an azimuthal mode order m and a radial mode order n [5].

2.1. Sources of sound

The mechanisms that generate acoustic modes in an axial compressor are several. Some of these sources are listed below:

1. rotor-alone mechanism,
2. rotor-stator interaction,
3. propagation of wakes and scattering,
4. flow separation.

Particularly, the phenomenon of scattering can be induced, for example, by a noticeably reflection of the propagating modes that can be scattered in other mode orders [9]. For a first study the resulting modes from wakes and flow separation will be neglected. Also the scattered modes are not taken into account but they can be analysed in the same way of the other modes.
The rotor-alone mechanism generates azimuthal mode orders m equal to integer multiples of the blades' number B [5]. To better understand this mechanism, a single rotor of an axial compressor is considered following the example in [12]. The spacing between the blades along the circumference is equal to $2\pi/B$ radians. Hence, the pressure contours associated

to a single blade should also repeat with this interval. Due to these considerations, the pressure distribution has to meet always two requirements [12]:

1. for a fixed coordinate system it spins with the angular velocity of the rotor $\omega = 2\pi N$, where N is the rotor shaft speed in cycle per second [cps];

2. it repeats in the period $2\pi/B$ defining the fundamental harmonic $h = 1$. Considering also the other harmonics ($h = 2, 3, 4, ...$) the repetition will be done with always smaller periods.

The sources of rotor-stator interaction noise are instead the following [12]:

1. Separation of wakes propagating from stators made by downstream rotor blades;

2. Impact of wakes generated from rotor's rotating blades on downstream stators;

3. Interference due to reflecting objects on the rotating periodic pressure field.

To explain the mechanisms that generates acoustic modes in this case of interaction, it can be considered a sequence of rotor blades rotating near a single stator vane as done in [12]. Near this vane it will be sensed a pressure fluctuation every time that a blade passes by. Alternatively, taking the position of a rotating blade a change in pressure will be sensed every time it approaches the vane. This fluctuation repeats every time that the blade completes a revolution and depends on the dimensions, position and aerodynamic influence of the vane [12].
In a fixed coordinate system near a vane this phenomenon is duplicated every time any other rotor blade passes by and thus takes place at blade passing frequency for every stator vane near the rotor [12].
This fluctuation is not sensed only near the vane, but it propagates along the duct [12].
Tyler and Sofrin verified that in a compressor stage with B rotor blades and V equally spaced stator vanes acoustic modes are created at harmonics of the Blade Passing Frequency (BPF) f_{BPF} [9]:

$$hf_{BPF} = hBf_R \tag{2.1}$$

where h is the Blade Passing Frequency harmonic $(1, 2, 3, ...)$ and f_R is the rotor turn frequency.
They demonstrated also that the m modes generated by interaction phenomena are given by the following expression [12][9]:

$$m = hB - kV, \tag{2.2}$$

where k can be equal to $\pm(1, 2, 3, ...)$. Otherwise, if $k = 0$ the corresponding m modes are that resulting from the rotor-alone mechanism.
For a particular harmonic h, the pressure field generated by rotor-stator interaction is composed of an infinite number of spinning modes, which have a value of m that comes from Eq.(2.2) as the index k assumes the value of all positive and negative integers [12].
Positive m numbers rotate in the same direction of the rotor whereas negative m in the

opposite. The spin rate of each m mode depends on its order as follows [5]:

$$\Omega_m = \frac{hB\omega}{m} \tag{2.3}$$

where Ω_m is the mode speed and ω is the rotor shaft speed.
The existence of the patterns given by the Eq.(2.2) can be demonstrated considering a compressor stage with few blades and vanes, as reported in [12]. The next figure illustrates in a schematic way the case of a rotor with number of blades $B = 8$ interacting with a stator with number of vanes $V = 6$.

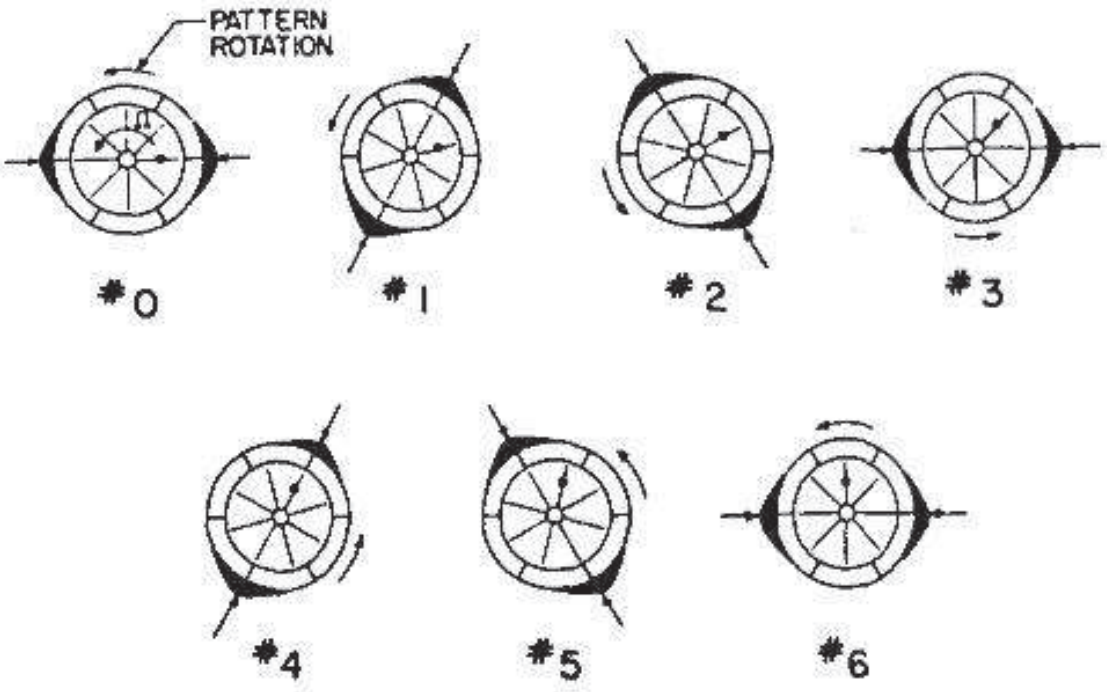

Figure 2.1.: Demonstration of rotor-stator interaction patterns. Taken from [12]

From Eq.(2.2) it can be derived that in this case, for example, the azimuthal mode order $m = 8 - 6 = 2$ occurs and from Eq.(2.3) that it is rotating at $\Omega_m = 8/2 = 4$ times the shaft speed ω. The rotor blades are represented by eight bars, one of which is marked with a large dot in order to follow the rotor position along its rotation. The six stator vanes are represented as short radial segments in the annulus around the rotor. In the first diagram, the marked blade coincides with the position of a stator vane and the same happens on the opposite side. The coincidences are highlighted by exterior arrows and the positive portions of the 2-lobe pattern are individuated by the black areas. The successive pictures show intermediate positions of the rotor during its rotation and all the coincidences that occur. Finally, in the last diagram, the rotor has made 1/4 of a turn whereas in this time interval the 2-lobe pattern has completed one whole revolution. It is therefore verified that the pattern is rotating at a rate of 4 times the rotor speed [12].

2.2. Propagation of sound in cylindrical ducts

In order to measure and control the noise produced, for example, by ducted fans, compressors and turbines but also to improve the structure's forced response prediction, it is important to understand the mechanisms of generation, propagation and interaction of acoustic modes in these ducts [2].
The propagation of the modes in the duct can be analysed considering the solution of the homogeneous wave equation. The boundary conditions at duct walls are needed in order to find this solution [5].
The following assumptions are made in order to derive the theoretical model, as done in the work of Tapken and Enghardt [10]:

- the medium is incompressible and the flow isentropic;
- the temperature and density are stationary in space and time whereas the temperature gradients are negligible;
- the boundary layer influences marginally the flow field for low axial Mach numbers, so the axial component of flow field does not depend on the radius;
- the duct section is constant along the axial direction;
- both axial and azimuthal mean flow profiles do not vary in axial direction and are also stationary in time;
- the radial flow component is neglected and the flow speed vector can be written as $\mathbf{U} = (U_x, 0, U_\Phi(r))^t$.

Particularly, the flow field can be described by two Mach numbers, the axial $M_x = U_x/c$ and the circumferential $M_\Phi = U_\Phi(r)/c = \Omega r/c$, which are both assumed to be well below one [10].
The equations on which the theoretical model is based are the continuity equation and the Euler equations, written using the cylindrical coordinates (x, r, Φ) [10].
From these equations, after some manipulations it can be derived the following general differential wave equation for the complex sound pressure p that describes the propagation of sound in ducts [10]:

$$\frac{1}{c^2}\left(\frac{D}{Dt}\right)^2 p - \Delta p = 0 \tag{2.4}$$

where Δ is the Laplacian operator. The material derivative D/Dt is defined as

$$\frac{D}{Dt} = \frac{\partial}{\partial t} + \mathbf{U}\cdot\nabla = \frac{\partial}{\partial t} + U_x\frac{\partial}{\partial x} + \Omega_s\frac{\partial}{\partial \Phi} \tag{2.5}$$

where ∇ is the Nabla operator in cylindrical coordinates.
For one frequency, the solution of Eq.(2.4) can be represented in the form of consecutive

series, resulting in a linear superposition of modes [10][9]:

$$p(x,r,\Phi) = \sum_{m=-\infty}^{\infty}\sum_{n=0}^{\infty}(A_{mn}^{+}\cdot e^{ik_{mn}^{+}x} + A_{mn}^{-}\cdot e^{ik_{mn}^{-}x})\cdot f_{mn}(r)\cdot e^{im\Phi} \tag{2.6}$$

where A_{mn}^{+} and A_{mn}^{-} are the complex amplitudes of the mode with azimuthal order m and radial order n for sound propagation in (+) and against (-) flow direction respectively.
If the acoustic boundary condition of hard walls is taken into account, the modes build an orthogonal eigensystem [10].

Radial distribution In Eq.(2.6) the term $f_{mn}(r)$ is called modal shape factor and defines how the shape of the mode varies along the radial direction. Its value is given by [10]:

$$f_{mn}(r) = \frac{1}{\sqrt{F_{mn}}}\left(J_m\left(\sigma_{mn}\frac{r}{R}\right) + Q_{mn}Y_m\left(\sigma_{mn}\frac{r}{R}\right)\right) \tag{2.7}$$

where J_m and Y_m are defined as the Bessel functions of first and second kind and order equal to the azimuthal mode order m. These functions are associated with σ_{mn} and Q_{mn}, that are the radial eigenvalues resulting from the boundary conditions of cylindrical hard walls [10].
An example of how the modal shape factor varies along the radius is depicted in the next figures where two low azimuthal mode orders ($m = 2$ and $m = 8$) and two high ones ($m = 178$ and $m = 196$) with the same radial mode order n are compared:

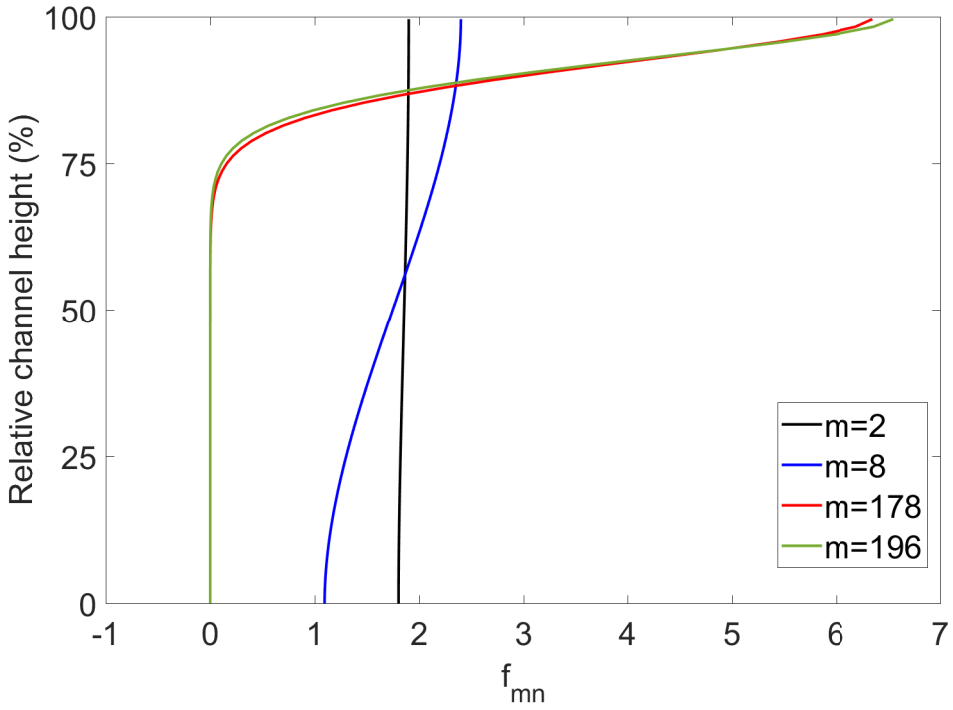

Figure 2.2.: Variation of the f_{mn} for different azimuthal mode order m and radial mode order $n = 0$

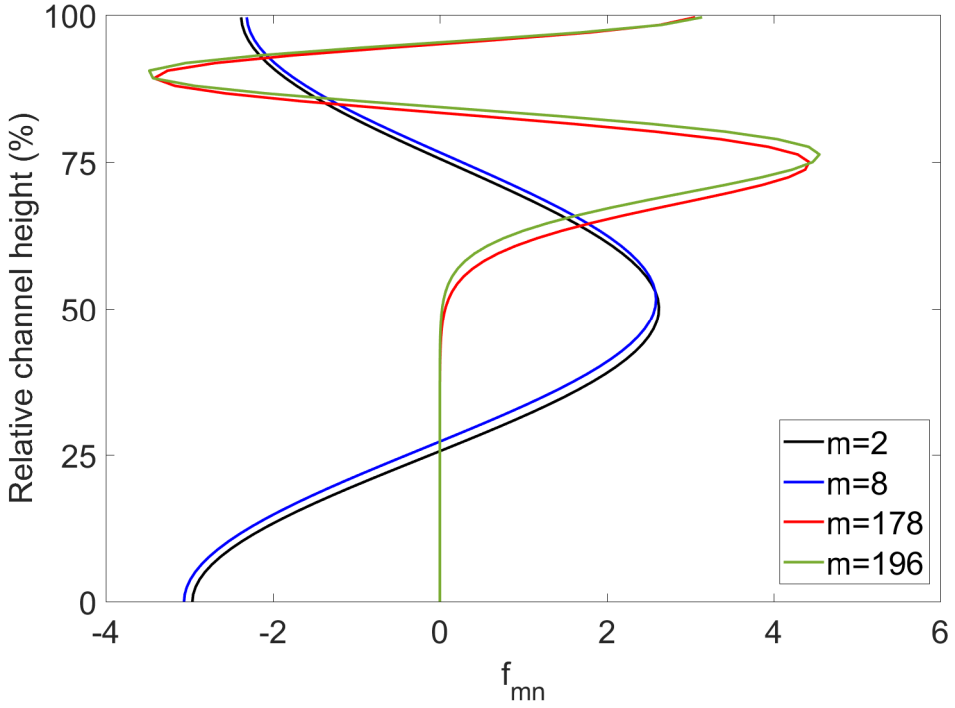

Figure 2.3.: Variation of the f_{mn} for different azimuthal mode order m and radial mode order $n = 2$

The eigenvalues σ_{mn} and Q_{mn} depend on the hub-to-tip ratio η, defined as follows:

$$\eta = \frac{R_i}{R} \tag{2.8}$$

where R_i is the inner duct radius and R the outer one.
The eigenvalues are determined from the equations that defines hard-walled acoustic boundary conditions. This means that the radial component of velocity of sound particle and the radial component of pressure gradient at the wall have to be zero, a condition necessary to insure the physical requirement of no airflow through the wall [9]:

$$r = R_i : J'_m(\eta\sigma_{mn}) + Q_{mn}Y'_m(\eta\sigma_{mn}) = 0 \tag{2.9}$$

$$r = R : J'_m(\sigma_{mn}) + Q_{mn}Y'_m(\sigma_{mn}) = 0. \tag{2.10}$$

Returning to Eq.(2.7), F_{mn} serves as a normalization factor and is defined through the integral [10]:

$$F_{mn} = \frac{1}{R^2}\int_{R_i}^{R} \hat{f}^2_{mn}(r) r\, dr \tag{2.11}$$

$$= \begin{cases} \frac{1}{2}[1-\eta^2] & m = n = 0 \\ \frac{1}{2}\left[\left(1 - \frac{m^2}{\sigma^2_{mn}}\right)\hat{f}^2_{mn}(R) - \left(\eta^2 - \frac{m^2}{\sigma^2_{mn}}\right)\hat{f}^2_{mn}(\eta R)\right] & otherwise \end{cases} \tag{2.12}$$

with

$$\hat{f}_{mn}(r) = J_m(\sigma_{mn}\frac{r}{R}) + Q_{mn}Y_m(\sigma_{mn}\frac{r}{R}). \tag{2.13}$$

The orthogonal mode eigensystem becomes through this normalization an orthonormal one.

Axial mode propagation Returning to Eq.(2.6), $k_{mn}^{\pm}$ are the axial wave numbers associated to the mode with azimuthal mode order m and radial mode order n. Their value depends on the mode eigenvalue σ_{mn} and the wave number for free field propagation k as follows [10]:

$$k_{mn}^{\pm} = \frac{k}{1 - M_x^2}(-M_x \pm \alpha_{mn}) \tag{2.14}$$

where

$$\alpha_{mn} = \sqrt{1 - (1 - M_x^2)\frac{\sigma_{mn}^2}{(kR)^2}}. \tag{2.15}$$

Considering the case in which the flow swirl does not occur, so that $M_\Phi = 0$, the wave number in free-field condition k is defined as follows:

$$k = \frac{\omega}{c} \tag{2.16}$$

where ω is the angular frequency of the rotor. Otherwise, if a swirling flow is imposed, the wave number in free-field condition k is modified as follows [10][9]:

$$\hat{k} = k - \frac{m\Omega_s}{c} \tag{2.17}$$

where Ω_s is the angular velocity of the component of the flow swirl. This modified wave number $\hat{k}$ has to be replaced instead of k in Eq.(2.14) and Eq.(2.15).
Depending on whether the axial wave number is real or complex, the propagation of the mode varies in one of two different ways along the x-axis, which ways can be derived from Eq.(2.6) considering the exponential term $e^{ik_{mn}^{\pm}x}$:

- If $k_{mn}^{\pm}$ is real, the mode propagates as a wave with constant amplitude in the form of a spiral along the duct until the end, radiating and producing far-field noise [12].

- If $k_{mn}^{\pm}$ has also an imaginary part, the modal amplitude decays exponentially as the axial distance from the source increases. This decay usually occurs in a very small distance and the mode can reach the end of the duct with negligible amplitude. [12].

In the first case, the mode propagates as a wave pattern rotating in a spiral way in the annulus like a helix [12]. In the developed view shown below, the pressure field is represented as a parallel wave propagating in a direction inclined to the x-axis of an angle θ which depends on the value of the circumferential Mach number M_Φ at which the pattern sweeps the annulus external wall and that is different for every single mode [12].

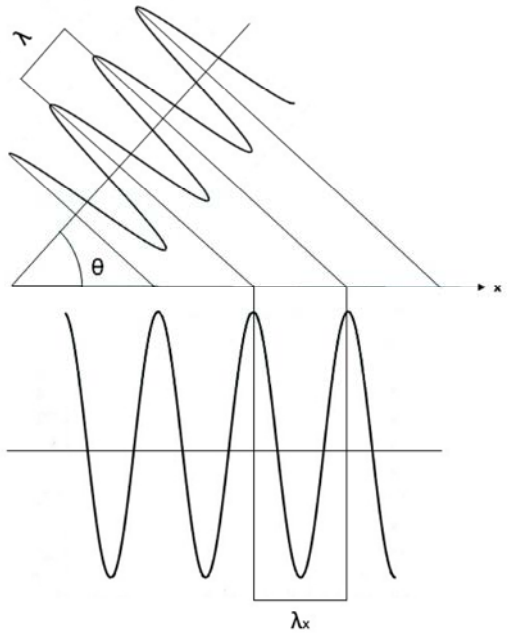

Figure 2.4.: Developed view to show the angle of propagation θ

Fig.(2.5) shows an example, taken from [9], of normalised acoustic pressure contours of the propagating modes with azimuthal mode order $m = 6$ and radial mode order from $n = 0$ to $n = 2$ in (+) and against (-) flow direction in a channel without hub shells.

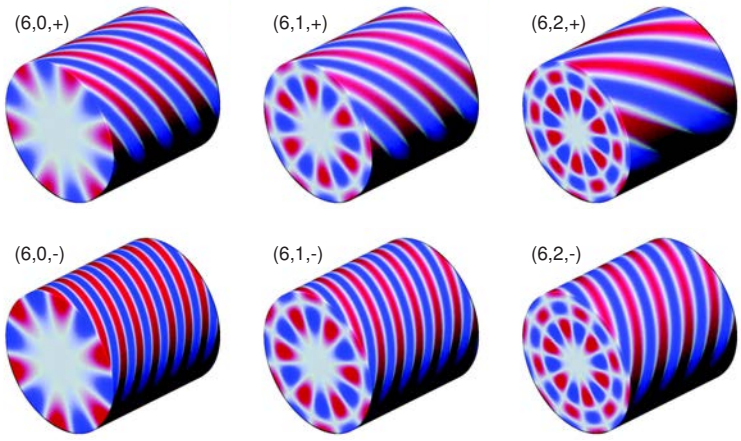

Figure 2.5.: Normalised acoustic pressure contours. Taken from [9]

From this plot it can be noticed that the propagation angle θ is different for every case. This consideration can be extended for every combination of azimuthal mode order m

and radial mode order n.
The angle θ between the wave's normal and the channel axis, can be computed by the dispersion relation, that describes the effect of dispersion in a medium on the properties of a wave travelling within that medium [9]. It comes from that the angle is related to the axial wave number, which is different for every (m, n)-mode, as it can be seen from Eq.(2.14).
In the case of $k_{mn}^{\pm}$ having also an imaginary part, the amplitude of the associated pressure decays exponentially along the x-axis according to the factor $e^{ik_{mn}^{\pm}x}$.
In order to have a reference measure on how fast the intensity of pressure can decrease with the distance, an example is reported, which considers two not propagating modes compared to a propagating one. The data used for making these plots are that of the successive analysis. Particularly, Fig.(2.6) shows the trend of the amplitude of the complex pressure associated to the mode whereas Fig.(2.7) in the next page only its real part.

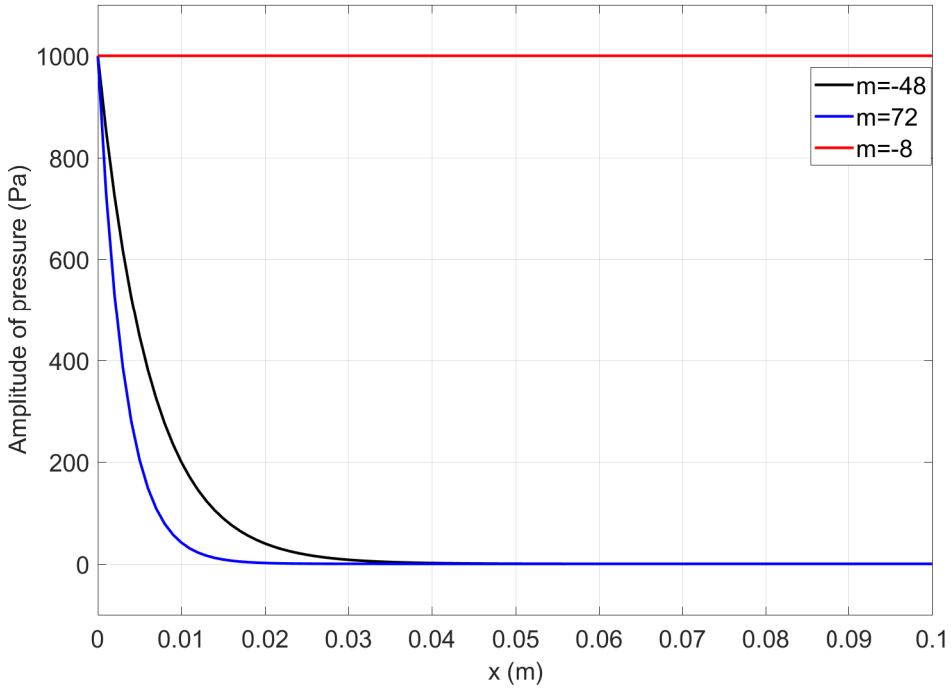

Figure 2.6.: Exponential decay of the amplitude of pressure created by the mode of azimuthal order -48 and 72 and radial order 0 compared to the undiminished amplitude of a propagating mode with m=-8 and n=0

In order to better understand the mechanism these plots are made considering a same modal amplitude for every mode and also a same phase. The modal shape factor has not been considered and also these plots refer to only one azimuthal position in the duct and one direction (+).
From these plots, it is clear that, for the non-propagating modes, the amplitudes of the pressure fluctuations decay only in a few centimetres and the decay rate is more high as the imaginary component of $k_{mn}^{\pm}$ increases, as happens in the case of the higher azimuthal mode order $m = 72$. The same consideration can be done for higher radial mode orders

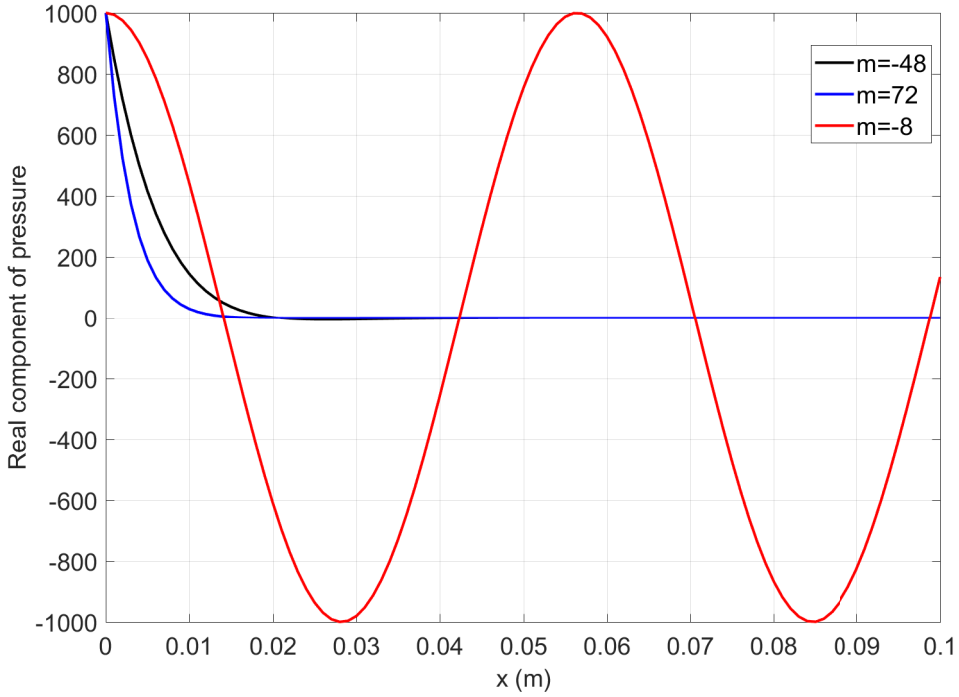

Figure 2.7.: Exponential decay of real component pressure created by the mode of azimuthal order -48 and 72 and radial order 0 compared to the propagation of mode with m=-8 and n=0

n of the same azimuthal mode order m.
Instead, like expected, the pressure due to the propagating mode $m = -8$ has a constant amplitude along the x-axis and propagates like a wave.
For a regular propagation of the mode the factor α_{mn} has to be real and this occurs when [9]:

$$k_0 R \geq \sqrt{(1 - M_x^2)}\sigma_{mn} =: (kR)_{mn} \tag{2.18}$$

where $(kR)_{mn}$ is called the cut-on frequency of the mode (m, n).

2.3. Solving the azimuthal and radial mode decomposition

Experimentally, the pressure field propagating along the duct is acquired using a measuring sensor array. The measured values are then adapted to a theoretical model describing this field [3].
Practically, the measuring grid often consists of one or more sensors circumferentially and radially traversed across the duct cross section for a minimum of two axial planes along the duct. In this way, the decomposition of the pressure field into azimuthal and radial mode orders can be implemented [4].

However, on the inlet section of a turbomachine, it is convenient to avoid the presence of probes immersed in the flow because the wakes generating from them would change the inlet flow conditions and also its acoustic characteristics [4]. An alternative arrangement of the sensor array has been developed in order to make measurements also in the inlet side and this arrangement consists of a series of sensors azimuthally mounted flush with the duct wall and equally spaced in the axial direction [6].
To separate the modes means to implement an azimuthal and a radial mode decomposition. An experimental technique is needed in order to calculate the amplitudes of all the modes, propagating or not, that occur in the duct [2].
Considering the series of Eq.(2.6) limited, this expression can be formulated as a system of linear equations and written in the following compact form [1][9]:

$$\mathbf{p} = \mathbf{W}\mathbf{a} \tag{2.19}$$

where $\mathbf{p}$ is the complex acoustic pressure vector, $\mathbf{a}$ the mode amplitude vector and $\mathbf{W}$ a matrix that contains all the other terms in Eq.(2.6). Particularly, each entry refers to a specific mode and sensor position.
The vector of complex pressure $\mathbf{p}$ can be described by [9]:

$$\mathbf{p} = (p(x_1, r_1, \Phi_1), p(x_1, r_1, \Phi_2), ..., p(x_{N_x}, r_{N_r}, \Phi_{N_\Phi}))^t \tag{2.20}$$

where $N_x \cdot N_r \cdot N_\Phi$ is the total number of measuring points considered.
The vector of the amplitudes of modes with azimuthal mode order m and radial mode order n is defined as [9]:

$$\mathbf{a} = (A_{0,0}, A_{0,1}, ..., A_{M,N})^t \tag{2.21}$$

where the subscripts refer to the order of modes as follows choosing the same notation used in [9]:

- azimuthal mode order: $0, 1, ..., M \sim min(m), min(m)+1, ..., max(m)$;
- radial mode order: $0, 1, ..., N \sim (0,+), (0,-), ..., (max(n),-)$.

Hence, the dimension of vector $\mathbf{a}$ corresponds to the number of modes considered in (+) and against (-) the flow direction.
The matrix $\mathbf{W}$ is built up as follows [9]:

$$\mathbf{W} = \begin{pmatrix} \Psi_{0,0}(x_1, r_1)e^{i0\Phi_1} & \Psi_{0,1}(x_1, r_1)e^{i0\Phi_1} & ... & \Psi_{M,N}(x_1, r_1)e^{iM\Phi_1} \\ \Psi_{0,0}(x_1, r_1)e^{i0\Phi_2} & \Psi_{0,1}(x_1, r_1)e^{i0\Phi_2} & ... & \Psi_{M,N}(x_1, r_1)e^{iM\Phi_2} \\ \cdot & \cdot & \cdot & \\ \cdot & \cdot & \cdot & \\ \cdot & \cdot & \cdot & \\ \Psi_{0,0}(x_{N_x}, r_{N_r})e^{i0\Phi_{N_\Phi}} & \Psi_{0,1}(x_{N_x}, r_{N_r})e^{i0\Phi_{N_\Phi}} & ... & \Psi_{M,N}(x_{N_x}, r_{N_r})e^{iM\Phi_{N_\Phi}} \end{pmatrix}. \tag{2.22}$$

The axial and radial eigenfunctions are contained in [9]:

$$\Psi_{m,n}(x_j, r_k) = e^{ik_{mn}^{\pm}x} f_{mn}(r_k). \tag{2.23}$$

The pseudo-inverse of matrix $\mathbf{W}$ can be used to solve the matrix equation in order to determine the parameters of interest, the radial mode amplitudes $\mathbf{a}$ [9]:

$$\mathbf{a} = [\mathbf{W^T W}]^{-1}\mathbf{W^T p} = \mathbf{W}^{+}\mathbf{p}. \tag{2.24}$$

The matrix $\mathbf{W}^{+}$ is called the pseudo-inverse of matrix $\mathbf{W}$.
There are different methods in order to solve the matrix system, but only two of them are used in the analysis and hence explained in subsections (2.3.2) and (2.3.3).

2.3.1. Partition of the system into an azimuthal and a radial mode analysis

Another way in order to solve Eq.(2.19) is to split the system, and hence the matrix, into two parts, one referred to only the azimuthal mode analysis and the other to the radial analysis of one single azimuthal mode order.
Later in this study, it will be implemented a radial mode analysis supposing that an azimuthal mode analysis is already completed. Eq.(2.6) can be written like [10]:

$$p(x, r, \Phi) = \sum_{m=-\infty}^{\infty} A_m(x, r) \cdot e^{im\Phi} \tag{2.25}$$

with

$$A_m(x, r) = \sum_{n=0}^{\infty} (A_{mn}^{+} \cdot e^{ik_{mn}^{+}x} + A_{mn}^{-} \cdot e^{ik_{mn}^{-}x}) \cdot f_{mn}(r). \tag{2.26}$$

The terms $A_m = A_m(x, r)$ are called azimuthal mode amplitudes and their values can be calculated thanks to a discrete Fourier transformation (DFT) in the azimuthal direction [10]:

$$A_m(x_0, r_0) = \frac{1}{N_\Phi} \sum_{l=0}^{N_\Phi - 1} p(x_0, r_0, \Phi_l) \cdot e^{-im\Phi_l}. \tag{2.27}$$

In order to complete the DFT it is necessary to measure the complex acoustic pressure values in the azimuthal direction with N_Φ equally spaced sensors at a constant axial and radial position (x_0 and r_0) [10]. Given a number of sensors N_Φ, there is an highest azimuthal mode order m_{max}, for which its amplitude can be determined univocally [10]. The value of m_{max} is given by the Nyquist theorem [10]:

$$\frac{1}{2}\frac{2\pi}{m_{max}} > \Delta\Phi = \frac{2\pi}{N_\Phi} \Rightarrow m_{max} < \frac{N_\Phi}{2}. \tag{2.28}$$

Hence, the spacing between the azimuthal sensors has to be lower than half of the wavelength $2\pi/m_{max}$ in order to find the amplitude of m_{max} without uncertainty [10].
For each azimuthal mode order m Eq.(2.26) can be written in the matrix form [10]:

$$\mathbf{A_m} = \mathbf{W_m} \cdot \mathbf{a} \tag{2.29}$$

where $\mathbf{A_m}$ is the vector of the measured azimuthal mode amplitudes of order m, $\mathbf{a}$ the vector of radial mode amplitudes and $\mathbf{W_m}$ the matrix with all the other factors in Eq.(2.26).

Particularly, each entry refers to a specific radial mode and sensor position. These quantities will be more in detail explained in Appendix A.
The same methods used for the entire system can be implemented in order to find the radial mode amplitudes **a**. Two of these methods are explained in the next two subsections.

2.3.2. Singular Value Decomposition

A way to calculate the pseudo-inverse of matrix **W** is the method of the Singular Value Decomposition (SVD). This method has the advantage that even if the matrix **W** is close to be singular an acceptable solution can be determined [9].
With the help of the SVD method the matrix **W** can be divided in [9]:

$$\mathbf{W} = \mathbf{U}[diag(\zeta_j)]\mathbf{V^T}. \tag{2.30}$$

The singular values ζ_j build up the principal diagonal of the square matrix $[diag(\zeta_j)]$. The matrices **U** and $\mathbf{V^T}$ are in this case orthonormal. The solution vector results from [9]:

$$\mathbf{a} = \mathbf{V}[diag(1/\zeta_j)]\mathbf{U^T}\mathbf{p}. \tag{2.31}$$

Particularly, the resulting vector of the mode amplitudes minimizes the functional [9]:

$$J = \|\mathbf{e}\|^2 = \|\mathbf{Wa} - \mathbf{p}\|^2. \tag{2.32}$$

The residuum $\|e\|^2$ includes the systematic and stochastic inaccuracies of the analysis [9].
The stability of the solution depends on the spectrum of the singular values. When one or more of the these are zero the matrix is singular and there is no solution [9].
As a relative evaluation measure for the stability of this numeric method the ratio of the highest singular value to the lowest, called condition number is used [9]:

$$\kappa = \frac{\zeta_{max}}{\zeta_{min}}. \tag{2.33}$$

A matrix is ill-conditioned when the condition number is so high that $1/\kappa$ approaches the zero.
The solvability and stability of matrix equation as well as the vulnerability of the system against noise is closely related to the condition number of the square matrix $\mathbf{W^T W}$ [9]. This assumption will be more clarified in the next chapter, considering Eq.(4.4).
Particularly, the singular values ζ_j, and hence the condition number, depend on various parameters: the number of modes, the frequency, the hub-to-tip ratio, the flow field and the chosen sensor arrangement [9]. This leads to the consideration that an optimization of the sensor array in order to keep the condition number relatively low is necessary to complete successfully the modal decomposition.

2.3.3. Orthogonal Matching Pursuit

The solution vector of the mode amplitudes **a** is called sparse when the entries of the vector are principally zero and, hence, when only few dominant modes occur in the duct.

In this case an approach in order to solve underdetermined systems of linear equations can be Compressed Sensing [1]. This method is based on the minimization of the l1-norm of the mode amplitude vector **a**, like follows [1]:

$$\mathbf{a} = argmin\|\mathbf{a}\|_1. \tag{2.34}$$

This expression has to satisfy the following relation [1]:

$$\|\mathbf{p} - \mathbf{W}\mathbf{a}\|_2 < \epsilon \tag{2.35}$$

where ϵ is the assumed noise energy.
A solution for the minimization problem can be found using the class of Greedy Algorithms, which find the best sparse approximation of the solution vector **a** through multiple iterations [1].
Particularly, in the analysis the Orthogonal Matching Pursuit algorithm (OMP) will be used. This method tries to find the dominant modes with the help of a convergence or stop criterion [1]. After a certain number of iterations the highest amplitudes of modes are contained in the mode amplitude vector **a** [1]. A particular characteristic of OMP is that at each iteration a mode is determined and its contribution is deconvolved from the acoustic complex pressure vector **p** [1].
Compressed Sensing offers the possibility to reduce the number of sensors in a circumferential array thanks to its performance of solving undetermined systems of linear equations [1].

3. State of the art

The study of acoustics in turbomachinery has been developing since the second half of the 20th century, when the problem of aircraft take-off exhaust noise becomes a concern in the airports areas. In 1962 Tyler and Sofrin provided a large contribution in this theme, publishing a paper on axial flow compressor noise [12]. Particularly, their work focuses on the discover of acoustic modes, which define the pressure field, and their generation, transmission along the duct and the consecutive radiation from the outlet. A prediction of which modes can be generated from the rotor-stator interaction is presented and demonstrated.
Ten years later Bolleter and Crocker introduced a method that determined the modal spectra of the first nine modes thanks to some measurements of pressure spectrum in the duct [2]. In the same year Moore studied the tones generated by an isolated rotor due to the interaction with flow distortions [7].
In 1987 Joppa published a paper in which a practical method for the pressure measurements is described and successfully tested [6]. This method consists of an array of microphones equally spaced along the circumference of the duct and mounted flush with the walls. Particularly, this work improved the linings design.
After almost ten years Heidelberg and Hall presented a new method for inlet acoustic mode measurements consisting of a continuously rotating microphone system. Other modes different from that expected from Tyler and Sofrin have been detected due to some disturbances [5].
In 2001 Rademaker, Sijtsma and Tester found a method in order to reduce the number of required azimuthal sensors [8]. This methods consists of the use and optimization of a randomly spaced array instead of an equally spaced one.
Some years later Enghardt, Tapken, Kornow and Kennepohl published a paper in which an alternative sound field model is derived considering a realistic radial flow profile instead of a uniform one usually used in the previous analytical models [3]. Then Tapken and Enghardt presented a study on the optimization of the measuring grid for a radial mode analysis [10]. In order to do this they focused on the quality of the analysis and on the factors that influences it. Four different measuring arrangements have been considered and compared.
In 2016 Behn, Kisler and Tapken presented a new approach for the azimuthal mode analysis based on Compressed Sensing [1]. This method is compared to the usual approaches. Also two ways of optimization of the circumferential array are introduced, which ways can decrease the number of required sensors only if the number of dominant modes is limited.

4. Process chain and optimization

The purpose of this study is to implement a mode decomposition in order to separate the radial amplitudes of the modes that occur in the channel starting from some discrete measurements of pressure in the duct. Because the stability of the analysis depends on the arrangement of the measuring grid, that can be designed directly by the user, a parameter study is done in order to optimize the grid parameters. Also the propagation of perturbations on the measured pressure into the system solution is studied during this optimization, based on the process in [10]. Fig.(4.1) illustrates the steps of the entire process:

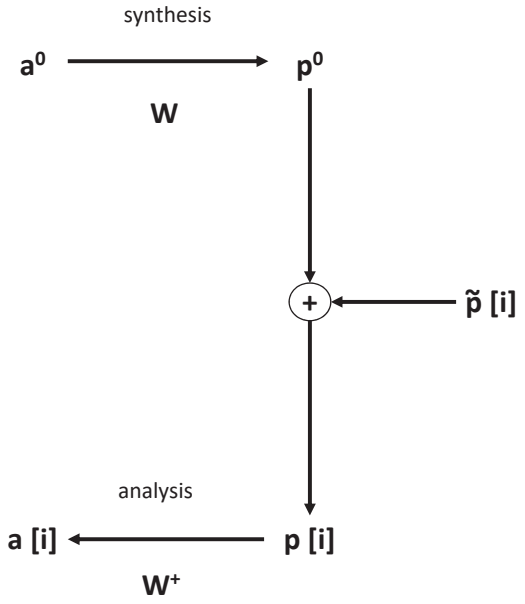

Figure 4.1.: Schematic illustration of the implemented process

This set-up is principally based on the work done by Tapken and Enghardt in [10] and the steps are here explained:

- the first step of synthesis consists of the calculation of the complex pressure vector $\mathbf{p^0}$ starting from a supposed vector of radial mode amplitudes $\mathbf{a^0}$. The entries of $\mathbf{p^0}$ contain the pressure values calculated through Eq.(2.6) for every measurement positions (x_j, r_k, Φ_l) with $j = 1, ..., N_x$, $k = 1, ..., N_r$ and $l = 1, ..., N_\Phi$;

- a noise perturbation $\tilde{p}$ is added to every element of vector $\mathbf{p^0}$. Particularly, this

operation is done for a number of i iteration in order to better evaluate the system stability;

- in the last step of the analysis the solution of the system, the radial mode amplitudes vector $\mathbf{a}[i]$, is calculated using Eq.(2.24) for every ith iteration. Particularly, the analysis ends successfully if the values of vector $\mathbf{a}[i]$ are close to that in the starting vector $\mathbf{a^0}$.

After N_{avg} iterations, the analysis quality can be evaluated using the relative error $\delta\mathbf{a}$ [9]:

$$\delta A = \frac{\overline{\|\tilde{\mathbf{a}}\|}/\|\mathbf{a^0}\|}{\overline{\|\tilde{\mathbf{p}}\|}/\|\mathbf{p^0}\|} \tag{4.1}$$

where:

$$\overline{\|\tilde{\mathbf{p}}\|} = \frac{1}{N_{avg}} \sum_{i=0}^{N_{avg}-1} \sqrt{\sum_{j=0}^{N_x-1} \sum_{k=0}^{N_r-1} \sum_{l=0}^{N_\Phi-1} |p(x_j, r_k, \Phi_l)[i] - p^0(x_j, r_k, \Phi_l)|^2} \tag{4.2}$$

and

$$\overline{\|\tilde{\mathbf{a}}\|} = \frac{1}{N_{avg}} \sum_{i=0}^{N_{avg}-1} \sqrt{\sum_{m=0}^{M} \sum_{n=0}^{N} |A^{\pm}_{mn}[i] - A^{\pm 0}_{mn}|^2}. \tag{4.3}$$

The relative error allows a more accurate evaluation of the analysis errors than the condition number, which only defines an upper limit on the possible error and satisfies the following relation [9][10]:

$$\frac{\|\tilde{\mathbf{a}}\|}{\|\mathbf{a}\|} \leq \kappa \frac{\|\tilde{\mathbf{p}}\|}{\|\mathbf{p}\|}. \tag{4.4}$$

It can be derived that $\delta A \leq \kappa$. From this expression it is seen that the condition number defines a maximum value of the instability of the equation system due to perturbations [10]. For example, if the condition number is equal to one, the relative amplitude variations in the solution are less or at most equal to the relative pressure perturbations [10]. Hence, introducing a pressure error equal to 5% the maximum radial amplitude error will be also equal to 5% [10].
An optimization of the measuring grid, which influences directly the accuracy of the results, like explained in subsection (2.3.2), is carried out looking for which number of sensors and distance between them these two quantities are minimized. This will be done in two separate analysis: the first considers the entire system in Eq.(2.19), so searches for an optimization for both azimuthal and axial positions, whereas the second uses the reduced system in Eq.(2.29), for which only an optimization for the axial array is needed since it is supposed that the azimuthal one is already completed.
The model has been entirely implemented using the software Matlab®.

4.1. Analytical superposition of acoustic modes

In this section the part of synthesis and, hence, the steps of programming a model for the analytical superposition of modes in a tube with different azimuthal and radial modal

orders at a constant radius along the channel axis is reported.
At the end the code will provide the value of the acoustic pressure due to this superposition in the considered measuring points located along the duct.
The calculation of this complex pressure refers to Eq.(2.6), that is the starting point of this analysis.
This first part of the process is summarised in the next illustration:

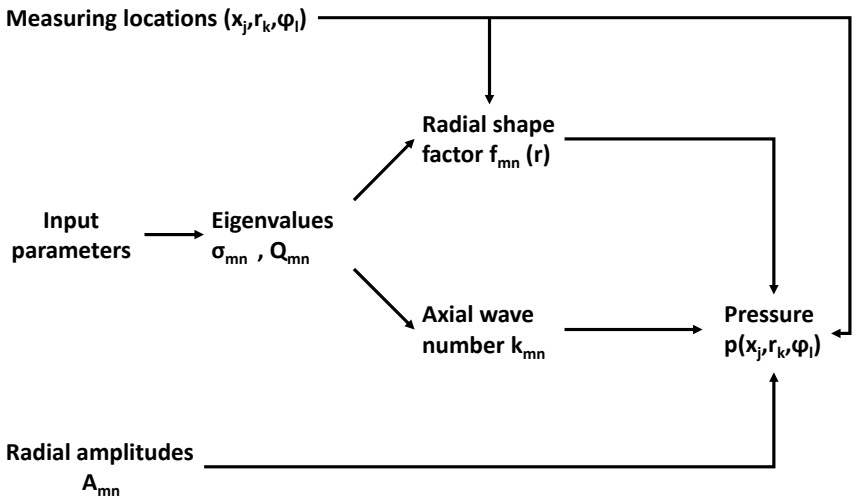

Figure 4.2.: Pressure calculation (step of synthesis)

The supposed input parameters are:

- how many and also which azimuthal and radial mode orders occur in the channel. In this general case the considered azimuthal mode order varies from -100 to 100 meanwhile the radial mode order from 0 to 10;

- the magnitudes of the complex amplitudes A^+_{mn} and A^-_{mn} for every mode of azimuthal order m and radial order n for sound propagation in and against flow direction respectively. From the previous experimental measurements and CFD simulations, it can be derived that the vector of these amplitudes is sparse, that means most of the values are zero or close to it;

- all the flow field characteristics like the axial Mach number at the tip radius M_x and the gas' temperature and composition (T and γ);

- the geometric and operative characteristics of the compressor like the hub and tip radius R_i and R, that together define the ratio η, the number of rotor blades B and that of stator vanes V and also the angular speed of the rotor ω.

The initial axial plane referred to the coordinate $x = 0$ is located close to the Inlet Guide Vanes and the measuring array extends from this point toward the inlet. All the characteristics of the compressor mentioned before are referred to a 2.5-stage axial compressor test rig located at the Institute of Jet Propulsion and Turbomachinery at RWTH Aachen University [11]. The next figure represents the sectional view of this compressor with simplified blade geometry and the line in red highlights the approximate location of the reference plane $x = 0$. The table below gives the number of blades and vanes for every component of the compressor.

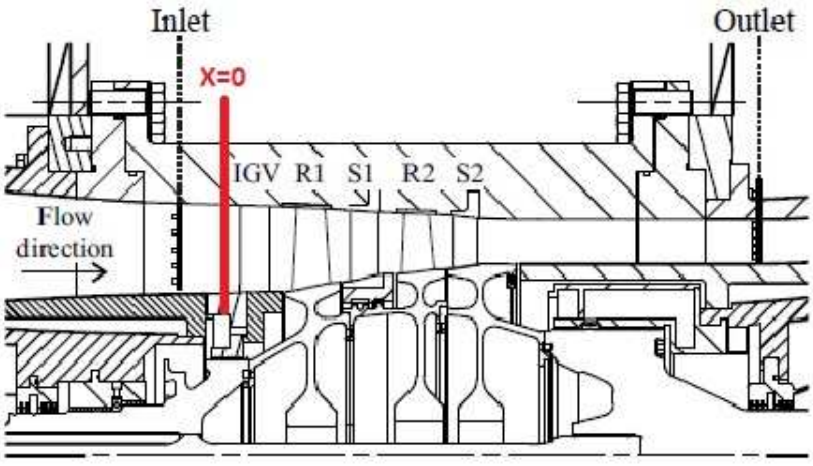

Figure 4.3.: Sectional view of the examined axial compressor. Taken from [11]

Row	IGV	R1	S1	R2	S2
Number of blades per row	40	32	52	38	70

Table 4.1.: Number of blades of the compressor components. Taken from [11]

A measuring array will be reproduced in the implementation of the code in order to simulate a real experimental set-up using the cylindrical coordinates (x, r, Φ).

4.1.1. Calculation of radial eigenvalues σ_{mn} and Q_{mn}

The first step in order to start this analysis is to calculate the eigenvalues σ_{mn} and Q_{mn} for every mode of azimuthal order m and radial order n. These eigenvalues will be after used to calculate the modal shape factors f_{mn} and the axial wave numbers $k^{\pm}_{mn}$ using respectively Eq.(2.7) and Eq.(2.14).

Like explained in subsection (2.2), these values come from satisfying the boundary conditions, which set the constraint of hard-walled acoustic duct. Mathematically two differential equations, Eq.(2.9) and (2.10), have to be solved. These equations contain the derivatives of the Bessel functions of first order J_m and of second order Y_m, which functions can be represented for different azimuthal mode orders like in the following figure:

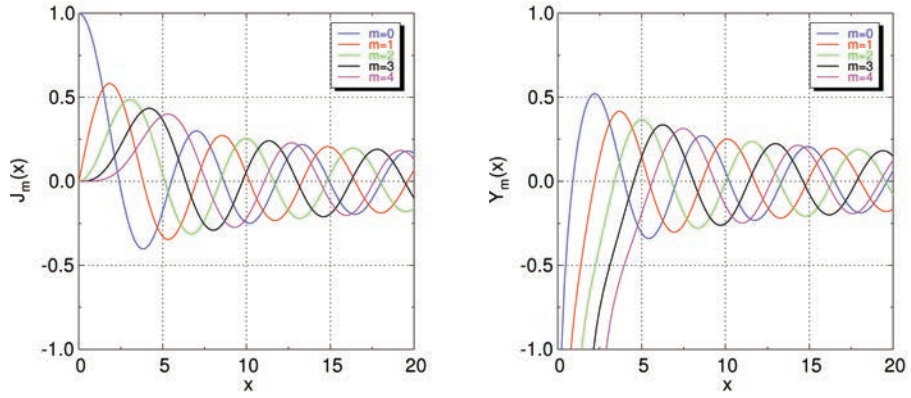

Figure 4.4.: Bessel functions J_m and Y_m of the azimuthal orders from 0 to 4. Taken from [9]

Particularly, the calculation of the eigenvalues in Matlab® has been made following two different paths that leads to the solution with a difference only in the computing time. The first and immediate method is to simply solve the differential equations Eq.(2.9) and (2.10) with the numeric solver named "*vpasolve*". Particularly, this command needs as input:

- the system of equations to be solved;
- the variables to solve the system of equations for, the eigenvalues σ_{mn} and Q_{mn};
- an initial guess close to the value of the solution.

The second method implies some manipulation of the differential equations that define the boundary condition, but its computing time is far less than the precedent one. From Eq.(2.9) and (2.10) the following relations can be derived (for the derivation see Appendix B). For $m = 0$:

$$J_1(\eta\sigma_{mn})Y_1(\sigma_{mn}) - J_1(\sigma_{mn})Y_1(\eta\sigma_{mn}) = 0, \tag{4.5}$$

$$Q_{mn} = -\frac{J_1(\sigma_{mn})}{Y_1(\sigma_{mn})} \tag{4.6}$$

and for $m > 0$:

$$\begin{aligned}&(J_{m-1}(\eta\sigma_{mn}) - J_{m+1}(\eta\sigma_{mn}))(Y_{m-1}(\sigma_{mn}) - Y_{m+1}(\sigma_{mn}))\\ &- (J_{m-1}(\sigma_{mn}) - J_{m+1}(\sigma_{mn}))(Y_{m-1}(\eta\sigma_{mn}) - Y_{m+1}(\eta\sigma_{mn})) = 0,\end{aligned} \tag{4.7}$$

$$Q_{mn} = \frac{J_{m+1}(\sigma_{mn}) - J_{m-1}(\sigma_{mn})}{Y_{m-1}(\sigma_{mn}) - Y_{m+1}(\sigma_{mn})} \tag{4.8}$$

For $m < 0$ the same equations are valid but the absolute value of m has to be considered. In order to find the values of σ_{mn} and Q_{mn} the numeric solver *vpasolve* is used like in the first method.
An arose issue for both methods is to find the initial guess which varies for every solution. The problem can be visualized plotting the function $y(x)$ corresponding to:

$$\begin{aligned}y(x) =&(J_{m-1}(\eta x) - J_{m+1}(\eta x))(Y_{m-1}(x) - Y_{m+1}(x))\\ &- (J_{m-1}(x) - J_{m+1}(x))(Y_{m-1}(\eta x) - Y_{m+1}(\eta x))\end{aligned} \tag{4.9}$$

that is exactly the left side of Eq.(4.7). The independent variable corresponds properly to $x = \sigma_{mn}$.
In the next figure the trends of function $y(x)$ for a low azimuthal order ($m = 2$) and a higher one ($m = 198$) are compared. In the first figure the entire image is plotted in order to see the difference of the magnitude order between the $y(x)$ of the two modes whereas below two zooms are done in order to better separate them and show the real trend of the curves compared to the first figure in which the fluctuations are not evident:

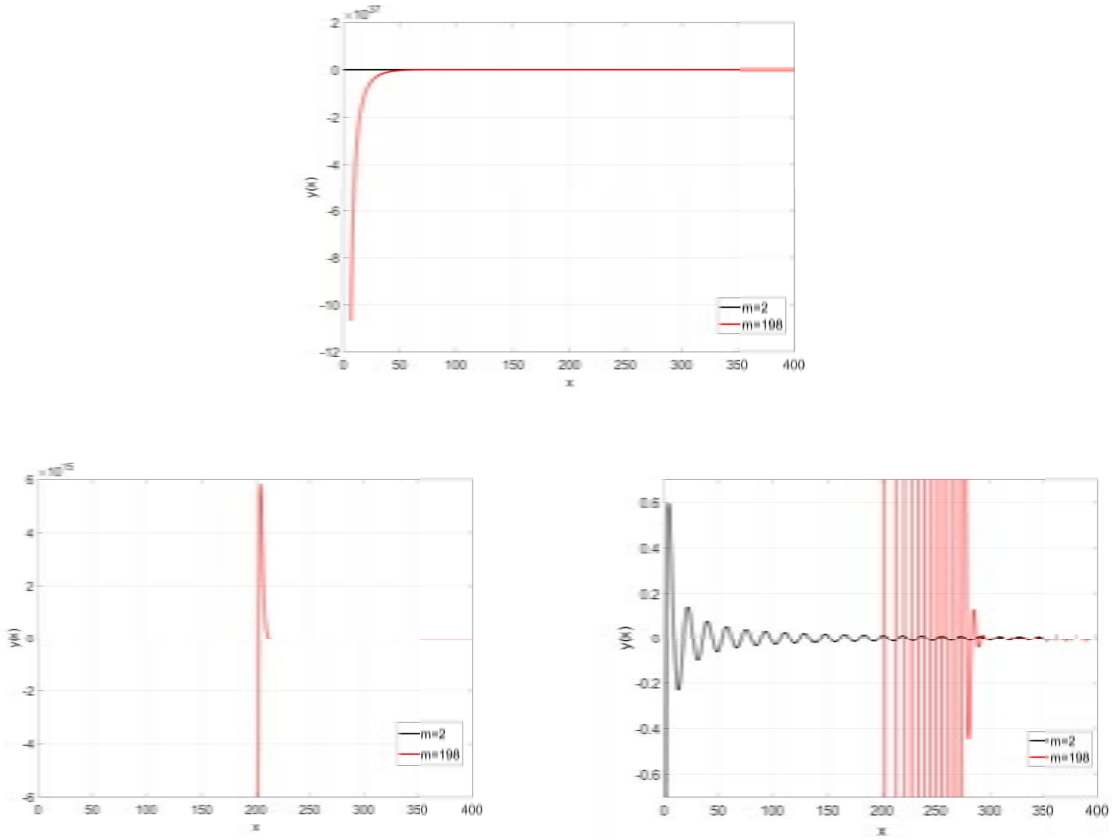

Figure 4.5.: Plot of the function $y(x)$ for the azimuthal mode order $m = 2$ and $m = 198$

Solving the system of equations corresponds to find the zeros of this function. The sequence of zeros corresponds to the ascending sequence of radial modal orders n for each different azimuthal mode order m. So, the first zero is linked to $n = 0$, the second to $n = 1$, and so on. It can be so derived that for every azimuthal mode order m there is an infinite number of solutions of Eq.(2.9) and (2.10) and each solution corresponds to only one value of the radial mode order n. This means that for every combination of m, n and η there is only one specific corresponding value of σ_{mn} and Q_{mn}.
These plots, made also for other values of azimuthal orders m, can be used to verify the finding of the right solution by the solver and also the accuracy of the method comparing the different solutions of σ_{mn} with the corresponding x-value in the plots.
The problem of finding the initial guess for every (m, n) combination can be understood looking at the trend of the function $y(x)$ in Fig.(4.5), which trend changes significantly as the azimuthal order m increases. For low values of m the points for which the function gets across this axis are more or less equally spaced and the gradient in the initial section is not very high. Otherwise, increasing m the amplitude gets higher and the function has an high gradient in the initial section. Hence, the "zeros points" are closer and this high gradient requires much more accuracy to find and check the values of x for which the function gets across this axis.
Comparing more plots and tables with yet obtained values it can be assumed that the σ with radial mode order $n = 0$ has always a value near to the absolute value of the considered m, so the initial guess is set to this value increased by 1 for every m. Concerning the Q, its initial guess is set to 0 for all the cases. The system is then resolved.
For the other ascending radial mode orders it has been found that adding 5 to the just previously calculated value of $\sigma_{m(n-1)}$ is a good choice for almost cases in order to find an initial guess for which the right σ_{mn} is calculated. The finding of the correct σ_{mn} is checked using plots as Fig.(4.5) for some combination of m and n. However, the right solution σ_{mn} is not always found at the first try but can consist of other three possibilities, summarised in the next figure with the subsequent steps to do:

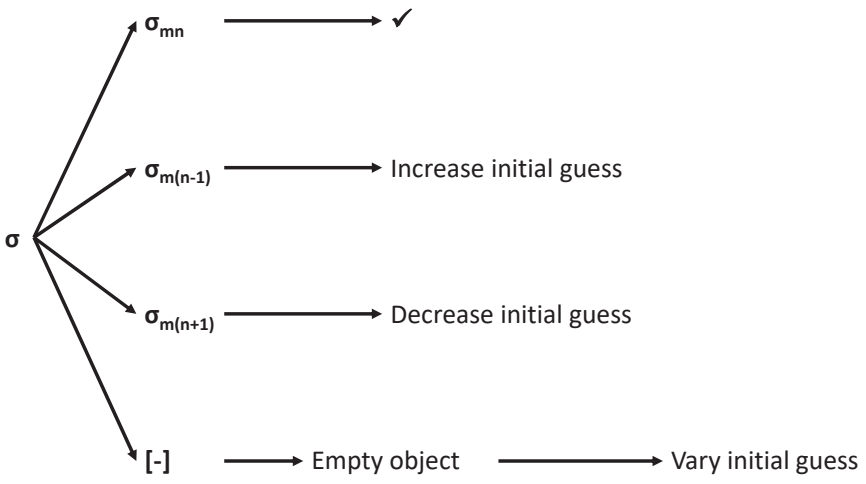

Figure 4.6.: Possibilities of solutions for σ_{mn} and subsequent steps

In the first case the solution is correct so also the initial guess value is, meanwhile in the other cases not. Particularly, in the second case the resulting value is equal to the previous solution. A check of this possibility is implemented in the process and, if it happens, the initial guess is increased by 2. This value has been found by trials and checking manually in order to find a value could fit for almost the cases. Instead, in the third case the starting value is too high and because of that the solver skips the solution of the considered radial mode order n. This is checked in the process seeing if the solution is too high in relation with the previous solution $\sigma_{m(n-1)}$. Hence, the initial guess is decreased by 2, that has always been found by trials. Finally, in the last possibility of empty object the initial guess is far from every solution. Hence, the starting value is increased by 2 and in the successive calculation the solution will corresponds to one of the previous possibility. The values to add or remove are found through several attempts in order to find the ones which could fit for every combination of m and n.
The check made in order to find if the solution is that corresponding to the considered radial mode order n and not the one corresponding to the previous or the next radial mode order has been verified manually not only using the illustrated plots but also changing the initial parameters and comparing the results to a given series of tested and verified values by Tyler and Sofrin.
Particularly, it has been checked that the final form of these methods gives the solution with an accuracy of minimum 10^{-4} to a maximum of 10^{-16} for some hub-to-tip ratio $\eta \geq 0.5$. This value of minimum accuracy is due to the fact that the published verified values from Tyler and Sofrin have this accuracy and that the manual check has not been carried out for all the considered combination of m and n for reasons of time (the calculated values are $M(= 201) \times N(= 11) = 2211$).

4.1.2. Calculation of pressure distribution

In the previous subsection the calculation of the eigenvalues and the consecutive arose problems are illustrated and explained. Considering Fig.(4.2), it can be seen that these values are needed to find the modal shape factors given by Eq.(2.7) and the axial wave numbers $k_{mn}^{\pm}$ given by Eq.(2.14) (if there is flow swirl, the free-field wave number is calculated using Eq.(2.17)).
The final step is the calculation of the pressure following Eq.(2.6).
Concerning the arrangement of the measuring grid, the input parameters that can be chosen and varied by the user are:

1. the number of axial, radial and azimuthal measuring points, that means N_x, N_r and N_Φ;

2. the distance between the axial measuring points and between the radial ones.

The characteristics of the implemented set-up are illustrated in the next figure:

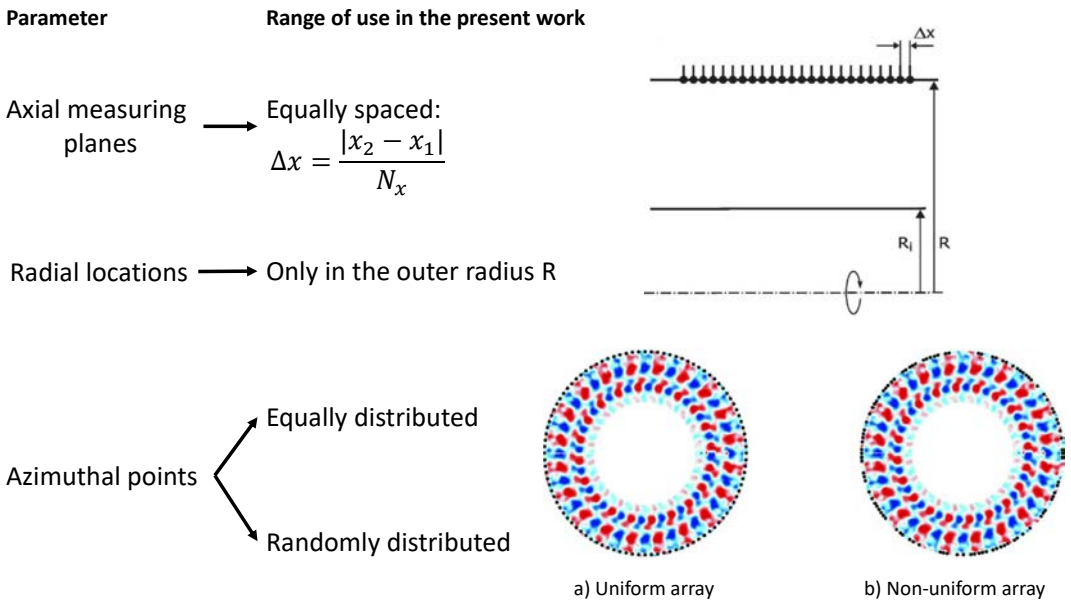

Figure 4.7.: Set-up of the measuring array. Images taken from [10] and [1]

First, the axial planes at which a circumferential array of sensors is located are assumed always equally spaced, like done in [9]; only the axial distance between them and the number can vary for every case. An equal spacing between the sensors is always done in practice because it has been found that is the best solution in order to search an optimized axial sensor separation. Referring to the figure, if x_1 is the starting point of the first axial plane, x_2 the x-coordinate of the last plane and N_x the number of axial planes, the spacing between them is equal to $\Delta x = |x_2 - x_1|/N_x$.
In the analysis, it is supposed that the starting plane has always coordinate $x_1 = 0$ and it is considered coincident with the reference plane highlighted in Fig.(4.3), which is near the Inlet Guide Vanes, so the axial planes are located in the negative direction of axis x going therefore from the IGV to the inlet.
Regarding the radial positions, like explained in section (2.3), sensors immersed in the flow would cause the change of the inlet flow conditions of the compressor and of its acoustic characteristic. Because of this, the probes are located only at the outer radius. Hence, in this case the number of radial measuring points N_r is always one.
Concerning the azimuthal measuring points, they can be equally or randomly circumferentially spaced according to needs. It is convenient that for every axial plane the arrangement of the azimuthal measuring points remains the same.
Finally, the calculation of pressure due to the superposition can be implemented using all these calculated input parameter and following Eq.(2.6).

4.2. Mode decomposition

In this section the set-up of an evaluation routine for the partition of azimuthal and radial modes by means of discrete circumferential measuring locations in different axial planes is reported at first. All this process consists of finding the solution vector of the radial mode amplitudes from Eq.(2.19) and looking for an optimization of the measuring grid which minimizes the values of the relative error δA and the condition number κ, whose expression are given respectively by Eq.(4.1) and Eq.(2.33).
Also the set-up made in order to solve the reduced system defined in Eq.(2.29), that comes after the split-up of the system into two separate analysis, the azimuthal and the radial, is illustrated. Particularly, in this second case only a radial mode analysis is implemented supposing that an azimuthal one is already completed. In this case the optimization concerns only the number of axial planes and the distance between them.
The implemented steps considering the whole system are illustrated below:

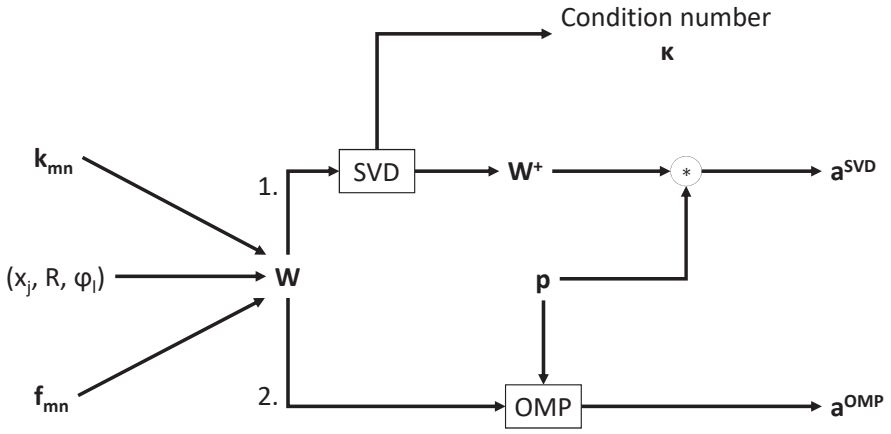

Figure 4.8.: Mode decomposition

All the procedure is based on the matrix equation (2.19). In order to find the vector of the mode amplitudes **a** from the vector of the measured complex pressure **p**, Eq.(2.19) can be inverted using the pseudo-inverse of matrix **W** according to Eq.(2.24).
In order to solve this matrix equation, the implemented method first builds up the matrix **W** as described in Eq.(2.22). Particularly, every column is referred to one combination of azimuthal mode order m, radial mode order n and direction (+ or -), whereas every row is referred to one measuring position. After the building of matrix **W**, the two methods described in subsections (2.3.2) and (2.3.3) are used in order to solve Eq.(2.19).
A particular attention regarding the minimum number of sensors necessary to solve the equation system has to be considered now.
The minimum number of the azimuthal measuring points N_Φ of an equally spaced array is

determined through the maximum value of the azimuthal mode order m using Eq.(2.28). Always from Nyquist theorem, it can be demonstrated that the number of the radial positions and the number of the axial planes have to satisfy the following relationship [9]:

$$N_x N_r \geq 2max(N_n(m)) \tag{4.10}$$

where $N_n(m)$ is the number of the radial mode order for that specific azimuthal mode order m. The factor 2 is needed for the determination of the radial modes in and also against the flow direction. Hence, the matrix system (2.19) is in practice in most of the cases overdetermined, that is the number of measuring position is higher than the number of the unknowns (the radial amplitudes of modes). Like it will be more in details shown in Ch.(5), a number of sensors really higher than the minimum leads to an analysis more stable and accurate.
The second method used in order to solve this azimuthal and radial mode decomposition is the Orthogonal Matching Pursuit algorithm. The idea behind this algorithm is explained in subsection (2.3.3). The input arguments of this algorithm are:

- matrix $\mathbf{W}$;
- the vector of measurements $\mathbf{p}$;
- the number of amplitudes that have to be detected.

Instead, the output arguments consist of the detected amplitudes vector $\mathbf{a}$. The results coming from both the SVD and OMP methods are evaluated and compared.

4.2.1. Parameter study

Like explained in subsection (2.3.2), the condition number and so the accuracy of the results depends on various parameters, but the easier and also the only for the user to change without modifying the flow conditions is the sensor arrangement. Because of this, an optimization regarding these following parameters has to be done in order to find accurately the complex modal amplitudes $A_{mn}^{\pm}$:

- the number of axial measuring planes;
- the distance between these axial planes;
- the number of azimuthal measuring points for every axial plane.

It is possible to find these values implementing a parameter study in which the following parameters vary:

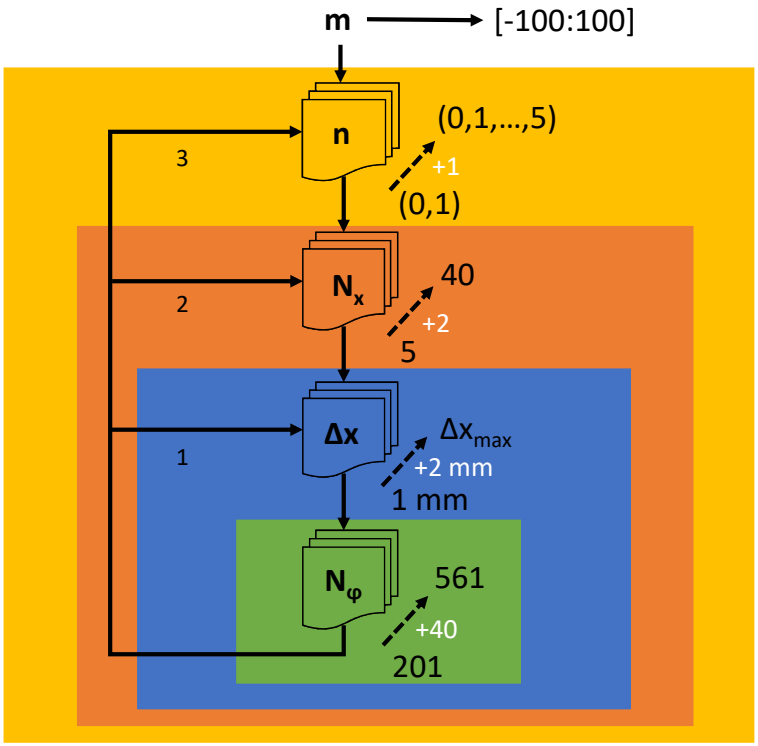

Figure 4.9.: Parameter study

The parameters are described below:

- n are the radial mode orders taken into account in the analysis and at every iteration a new one is added until the reaching of $n = (1 : 5)$;
- N_x is the number of axial planes increased by 2 at every iteration;
- Δx is the distance between the axial measuring planes. The value of Δx_{max} comes from a consideration that will be done below;
- N_Φ is the number of azimuthal sensors for every axial plane and they are increased by 40 at every iteration.

The analysis is done for every single combination of these values in order to find the optimal parameters. Particularly, every time that all the values of a quantity have been considered, the next value of the precedent parameter is taken into account and the analysis is repeated. The considered azimuthal mode orders m consist of all the values contained in the interval $[-100, 100]$, but, like mentioned at the beginning of section

(4.1), from previous measurements it has been found that most of the modes have an amplitude close to zero. Particularly the azimuthal mode orders m that have a not negligible amplitude correspond to that resulting from Eq.(2.2), that is $m = hB - kV$, in which the parameters assume the following values:

- $h = 1$ (first harmonic);
- $B = 32$, the number of blades of the first rotor as given in Table (4.1);
- k varies in order to stay in the interval [-100,100];
- $V = (40, 52)$ corresponding respectively to the number of vanes of the IGV and of the first stator as given in Table (4.1).

4.2.2. Discussion of the arose issues during this radial mode analysis

In a first try, the pressure error $\tilde{p}$ is not added to the system. However, even without error, some issues come out from this first analysis. The principal issue is due to the exponential form $e^{ik^{\pm}_{mn}x}$ in Eq.(2.6) and the imaginary component of $k^{\pm}_{mn}$ of the not propagating modes, which component increases as the azimuthal mode order and the radial mode order increase. Particularly, the problem is that after a certain small distance the entries of matrix $\mathbf{W}$ reach really high values toward the infinity and so compromising the stability of the system. This influences the complex pressure, that results in not physically reasonable values.
A way in order to avoid this reaching of infinity is to limit the axial expansion of the measuring array to a certain value x_{max}, for which corresponds the distance between the axial planes Δx_{max} in Fig.(4.9). Over x_{max}, the exponential term reaches the infinity value and so the analysis cannot be completed. However, even with this conditions, most of the solution are not correct because the condition number is still very high.
Also the big size of the matrix can be a problem for the stability of the method. In addition, because of the equal values of the parameters $k^{\pm}_{mn}$ and f_{mn} for the azimuthal mode order $+m$ and $-m$ the columns corresponding to this values will be also similar and this influences badly the stability of the matrix.
Particularly, for most combinations of parameters, the SVD method provides amplitudes of the non propagating modes which are 4-5 orders of magnitude higher than the amplitudes at the input. Because of this reason, the alternative method of OMP has been used in order to find another way of solution better than the SVD, but in this case, some particular modes, like for example $(m, n) = (32, 0)$, are not found for most of the analysis. Only for some combinations of the grid parameters the solution is found accurately. However, choosing for example a number of axial planes, the distance between them for which the correct solution is found changes according to the number of azimuthal sensors. Considering another number of axial planes, the values of distances change again always according to the number of azimuthal position. In addition, increasing the number of modes taken into account and so the size of the matrix $\mathbf{W}$, these good combinations of grid parameters changes again. Because there is the practical need to see if a grid with

some particular values of parameters experimentally can be set up, an optimization of all the parameters requires an accurate mathematical inquiry and a long period of time to find if there exist some general ranges in which operate practically.
In order to clarify the issues and simplify the problem, the optimization can be split up in two parts, the one concerning the axial planes and the one concerning the azimuthal measuring points. Supposing that an azimuthal mode analysis has already carried out, a degree of freedom, N_Φ, is removed from the system. Hence, the optimization looks if there is a range of distances between the axial planes that can be good for a large range of number of axial planes and also of number of modes.

4.2.3. Split of the system into an azimuthal and a radial mode analysis

Because of the issues illustrated in the previous subsection, the work focuses now only on the radial mode analysis, and hence, only in the optimization of the axial sensor array. The azimuthal mode analysis is supposed to be completed, so the azimuthal measuring positions are already optimized. However, because errors due to measurements inaccuracies and noise still occur, a perturbation on the azimuthal mode amplitudes is still added and its propagation into the system still studied, like in the previous analysis.
Particularly, instead of the complex pressure the azimuthal complex amplitudes A_m are computed according to Eq.(2.26). The general scheme in Fig.(4.1) is modified as follows:

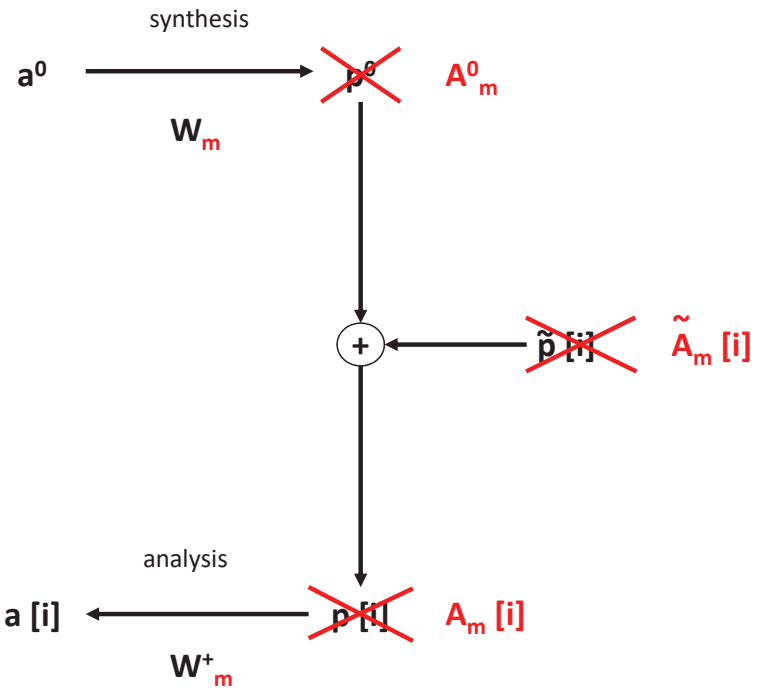

Figure 4.10.: Schematic illustration of the process for the radial mode analysis

All the quantities in the figure refers to only one azimuthal mode order, like the subscript

m suggests.
Particularly, this time the analysis has been carried out for two frequencies, the fundamental and for the second harmonic. Also, the considered values of the azimuthal mode order m are those expected for sure from the mechanism of the first rotor alone and from the interaction of the first rotor with the IGV and with the first stator according to Eq.(2.2). The values of the parameters used in this equation are already listed in subsection (4.2.1), with the difference that also $h = 2$ is considered for the frequency corresponding to the second harmonic. From these expected modes only the ones included in the interval $[-100, 100]$ has been considered. Particularly the azimuthal mode orders obtained are:

1. $m = (-88, -72, -48, -20, -8, 32, 72, 84)$ for the first harmonic;

2. $m = (-96, -92, -56, -40, -16, 12, 24, 64)$ for the second harmonic.

For every single mode order m, the process illustrated in figure (4.10) has been implemented.
In order to make an analysis independent from the specific values of the amplitudes, the ones of the vector $\mathbf{a}$ are set all equal to 1000 Pa with a random phase.
Another consideration about the not propagating modes is done pointing out that, like it can be seen in Fig.(2.6), they decay really fast in some centimetres. Hence, when they are to be reflected at the inlet coming from the IGV they will have a negligible amplitude. Assuming no scattering, also the amplitudes of the reflected modes and its associated pressure can be reasonably neglected.
This assumption assures to have lower condition numbers and so more stability in the system. Indeed, it is exactly with their combination of exponential, axial wave number and sign e^{ikx} that the entries of matrix $\mathbf{W}$, and hence the pressure, increase exponentially very fast according to the distance from the point of view of the IGV. The reached values are physically too high, in contrast with the consideration done before of the negligible amplitude. An example of the values that the reflected pressure can reach mathematically without the assumption done before is reported in Fig.(4.11), in which the trend of the pressure amplitude of not propagating reflected modes (direction +) is plotted for the azimuthal mode order $m = -48$ and $m = 72$ and the radial mode order $n = 0$.
From the position of the IGV, the pressure increases exponentially and the rate of the increment is higher as the azimuthal and radial mode number increase. This values are physically not reasonable because a not propagating mode hardly arrives at the inlet with that values of amplitude and then is reflected.
In a first analysis also the reflected propagating modes are neglected in order to compare the results with a second analysis in which only the reflected not propagating are neglected.
Concerning the methods in order to solve the system, the OMP algorithm is no longer be used because the vector of amplitudes is not sparse in this case.
The set-up of the parameters for the analysis and optimization is illustrated in Fig.(4.12).

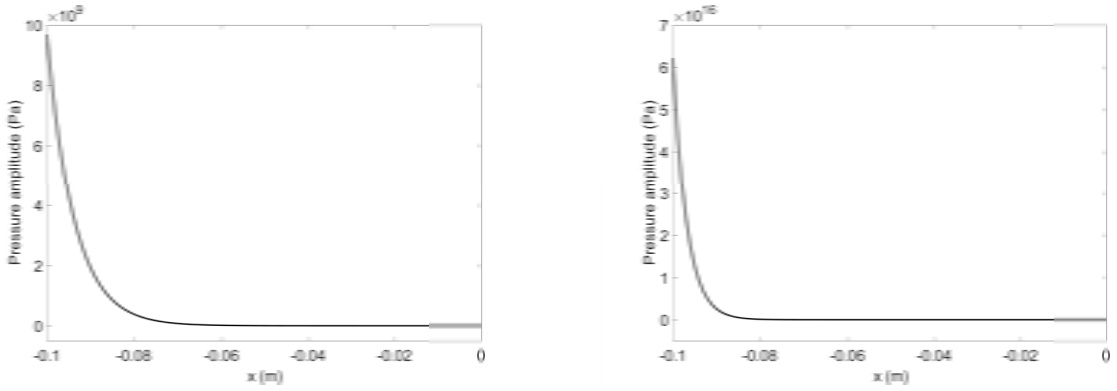

Figure 4.11.: Plot of the decay of the reflecting modes of azimuthal mode order $m = -48$ (in the left) and $m = 72$ (in the right) and radial mode order $n = 0$

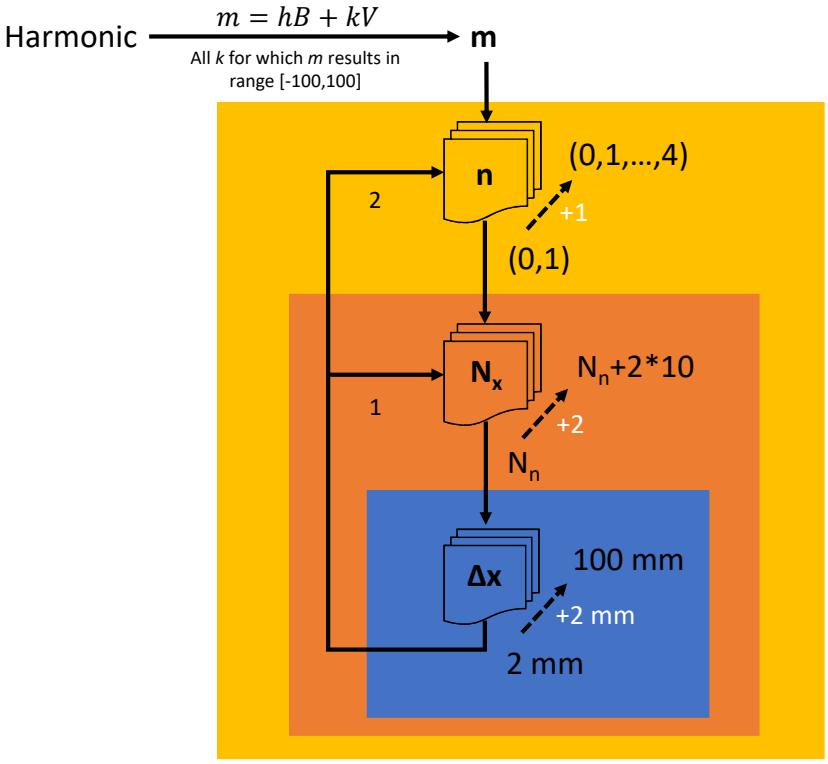

Figure 4.12.: Parameter study

Comparing this figure with the parameter study in Fig.(4.9) the number of azimuthal measuring points has been properly removed. Considering the axial planes, their number vary from the minimum value N_n obtained from Eq.(4.10) to a maximum number, making

the system overdetermined.
Particularly, one single analysis is repeated $i = 20$ times, in order to calculate the relative error δA. The expression of this error is properly modified from Eq(4.1) as follows [9]:

$$\delta A = \frac{\overline{\|\tilde{\mathbf{a}}\|}/\|\mathbf{a^0}\|}{\overline{\|\tilde{\mathbf{A}}_\mathbf{m}\|}/\|\mathbf{A^0_m}\|} \tag{4.11}$$

where:

$$\overline{\|\tilde{\mathbf{A}}_\mathbf{m}\|} = \frac{1}{N_{avg}} \sum_{i=0}^{N_{avg}-1} \sqrt{\sum_{j=0}^{N_x-1} |A_m(x_j)[i] - A^0_m(x_j)|^2} \tag{4.12}$$

and

$$\overline{\|\tilde{\mathbf{a}}\|} = \frac{1}{N_{avg}} \sum_{i=0}^{N_{avg}-1} \sqrt{\sum_{n=0}^{N} |A^{\pm}_{mn}[i] - A^{\pm 0}_{mn}|^2}. \tag{4.13}$$

Every time also the maximum error in amplitude and phase has been calculated and at the end the maximum of all these values is considered into account. The entire process has been carried out for three different types of perturbations $\tilde{A}_m$. Considering the expression of the initial azimuthal mode amplitude $A^0_m = a^0_m e^{i\Phi^0_m}$, the three different types have these expressions:

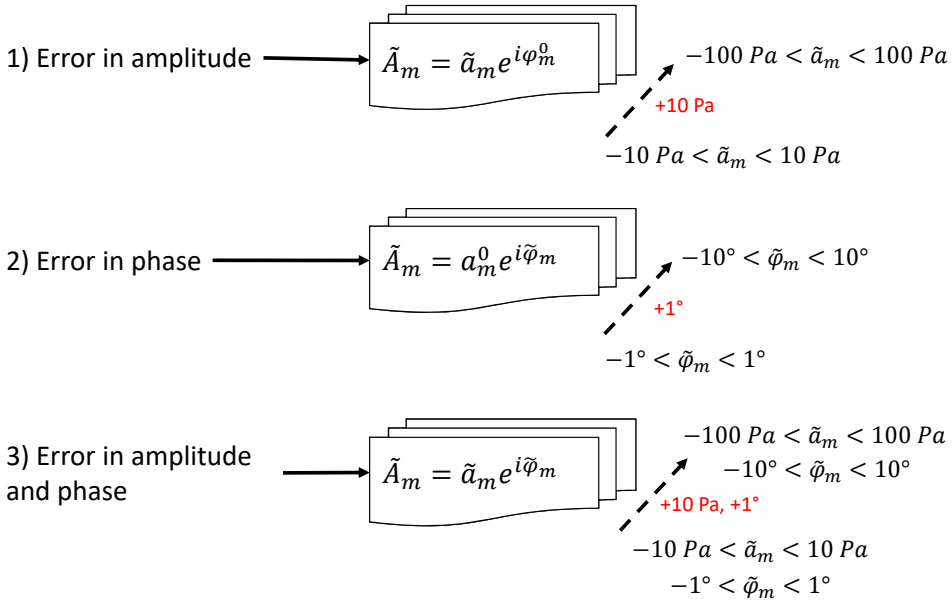

Figure 4.13.: Variations of the perturbations added to the system

For each type, the error has been introduced gradually and is different for every measuring position, like a noise effect. For example, for the first try in the case of only perturbation

in amplitude, the amplitude of this perturbation is included in the interval $[-10, 10]Pa$ whereas in the second in the interval $[-20, 20]Pa$ and so on, adding 10 Pa until the interval is $[-100, 100]Pa$.
Also an initial try where the perturbation is zero (ideal case) has been made for all the analysis, leading to a correct determination of all the amplitudes.
The results from all these analysis are displayed and discussed in the next chapter.

5. Final results and conclusions

In this chapter the results of the analysis, the process of which is explained in Ch.(4), are visualized and discussed. The base case for which the discussion of the results starts is referred to the design point, the first harmonic and only propagating modes. In this base case all the reflected modes are neglected and only an error in the amplitudes of the azimuthal mode amplitudes is added to the system. Starting from this base case, some of the mentioned parameters are changed and taken into account in order to study their influence on the analysis.
Particularly, in order to have an index of the analysis quality three quantities are studied:

- the condition number κ of matrix $\mathbf{W}$ given by Eq.(2.33);
- the relative error δA calculated through Eq.(4.11);
- the maximum absolute error in amplitude and phase calculated from the elements $A_{mn}^{\pm}$ in the vector of radial amplitudes $\mathbf{a}$.

The values of these quantities resulting from the analysis are elaborated in order to visualize some plots in which the optimization of the measuring grid is based. The optimized values of number of axial planes, N_x, and the distance between them, Δx, are to find visualizing where the quantities mentioned before are as low as possible.
The plots of δA and κ are made depending on the number of axial planes N_x and on the distance Δx between two of them. Choosing a number of axial planes, the maximum error in amplitude or phase of the radial mode amplitudes is depicted depending on the maximum error $\tilde{A}_m$ added to the system and on the distance between two axial planes.
Different cases in which some assumptions and conditions of the analysis vary are compared. Particularly, the results coming from the cases in Fig.(5.1) which the mentioned parameters vary can be discussed.
From now on all the considered azimuthal mode orders m are that listed in subsection (4.2.3) coming from Eq.(2.2).

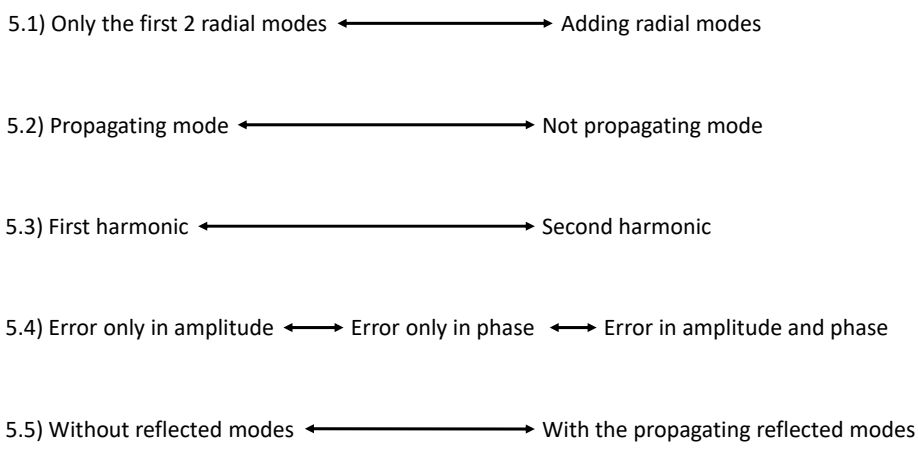

Figure 5.1.: Different comparisons of the results

5.1. Effects of adding radial mode orders into account

First it will be illustrate the results for $m = -8$, which for the considered operative conditions is propagating with all the radial mode orders from $n = 0$ to $n = 4$. The mode occur at first harmonic and for now, only an amplitude perturbation in the azimuthal mode amplitudes A_m is considered, as shown in the first case of Fig.(4.13). The reflected modes coming from the inlet are for now neglected. This case corresponds to the base case illustrated at the beginning of this chapter.
Particularly, the evolution of the relative error δA and the condition number κ when radial modes are added into the analysis is discussed at first. The maximum perturbation on the azimuthal mode amplitudes for which these plots are made is 10 Pa. However, it has been checked that increasing the maximum error has a very small influence on δA because it is a relative measure. Also, increasing the perturbation on A_m has no influence of the condition number κ because it is independent from the errors and it defines only a measure of the condition of the matrix. In all the plots in dark red are displayed the results that are equal or greater than the last value of the colorbar. The values of y-axis change according to the number of radial modes taken into account because the analysis starts from the minimum number of axial planes N_n given by Eq.(4.10).

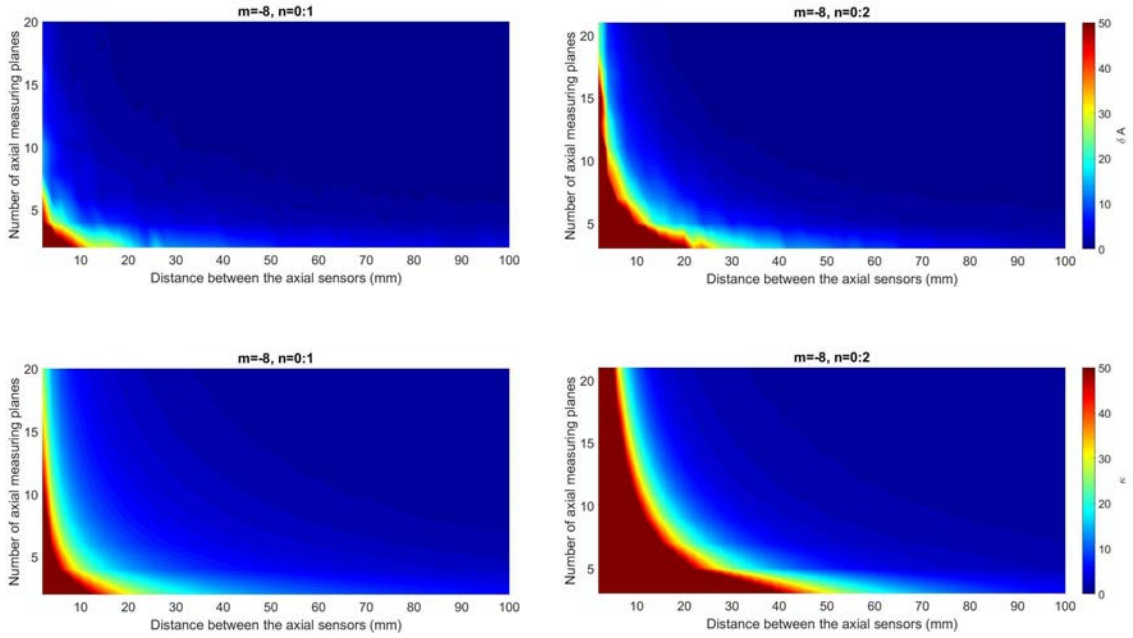

Figure 5.2.: Comparison of δA and κ for $m = -8$ and $n = (0, 1)$ (in the left) and $n = (0, 1, 2)$ (in the right)

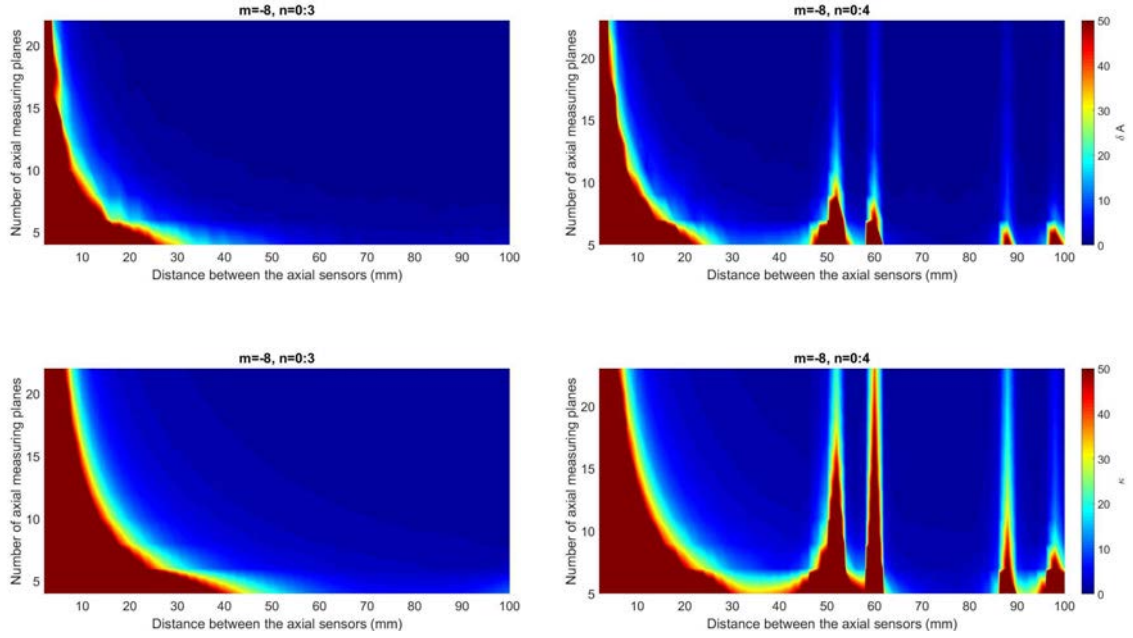

Figure 5.3.: Comparison of δA and κ for $m = -8$ and $n = (0, 1, 2, 3)$ (in the left) and $n = (0, 1, 2, 3, 4)$ (in the right)

From Fig.(5.2) and (5.3) it can be seen that for the first three cases the values of δA and κ decrease as the number of axial planes and the distance increase, implying a better condition and stability for the matrix $\mathbf{W}$ and the entire analysis. Increasing the number of planes, the distance between them can be decreased. Particularly, adding gradually a radial mode order into account the minimum value of distance for which the values of δA and κ stay low for a specific number of axial planes increases. A reason for this trend could be that the axial wave number k_{mn} decreases as the radial mode order n increases and this influences the wavelength of the mode which becomes higher, requiring so an higher spacing between the axial sensors in order to be detected with accuracy.
Considering also the radial mode order $n = 4$, the ranges of distances between the planes in which the two values stay low are not only the small ones but vary depending on the number of axial planes. Particularly, the increase of number of planes helps the enlargement of these ranges of distance. For $N_x >> N_n$ almost all the distances can be chosen for an optimization except for the very small ones ($\Delta x < 10\ mm$).
For every case it is demonstrated that $\delta A \leq \kappa$, like stated at the beginning of Ch.(4).
The same considerations can be done also for the other propagating m modes, with the difference that, in a checked range, increasing the number of m but always considering the propagating ones, the values of δA and κ are respectively lower for most of the combinations of N_x and Δx.

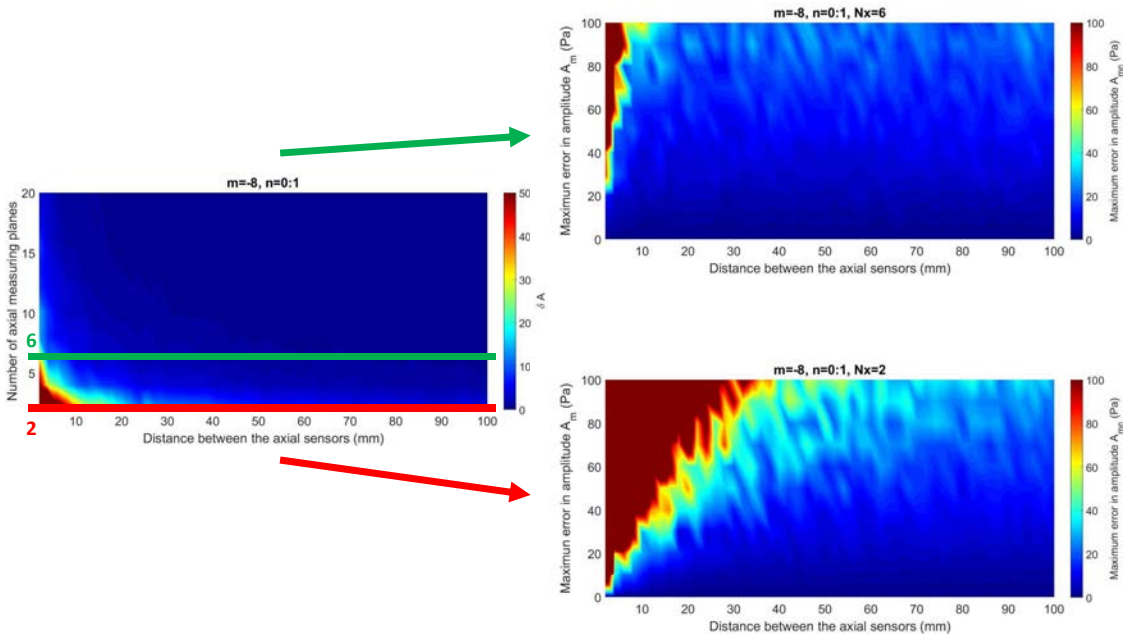

Figure 5.4.: Comparison of maximum errors in the amplitudes of A_{mn} for $m = -8$ and $n = (0, 1)$ increasing N_x

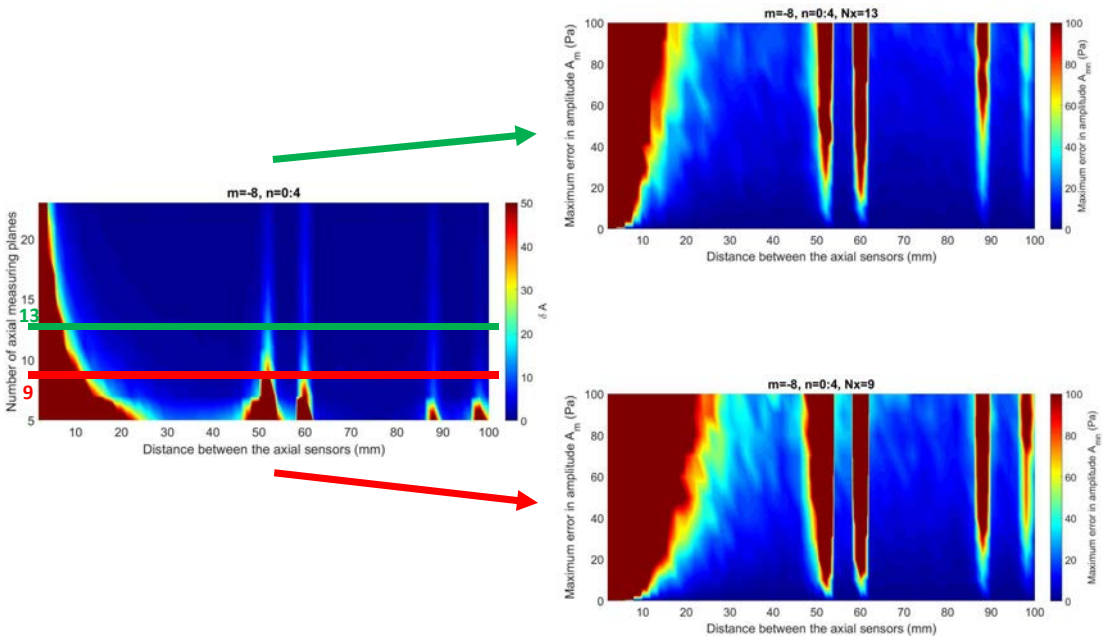

Figure 5.5.: Comparison of maximum errors in the amplitudes of A_{mn} for $m = -8$ and $n = (0, 1, 2, 3, 4)$ increasing N_x

In Fig.(5.4) and (5.5) the maximum error in the amplitudes of the radial amplitudes chosen from all the repeated simulations of the same analysis is plotted. This error depends on the maximum perturbation in amplitude added to the system and on different distances between the axial planes. Particularly, in Fig.(5.4) there is the case of the first two radial modes, whereas in Fig.(5.5) the case of all the considered radial modes. Two plots of the maximum errors are made, which are referred to a different number of axial planes N_x in order to evaluate the positive effect of increasing them like noticed in δA and κ.
Taken the horizontal line in the plot of δA corresponding to the considered number of axial planes it can be noticed that the ranges in which δA and κ become higher corresponds to the ranges in which the perturbation on the azimuthal amplitudes influences negatively the solution of the radial amplitudes, like expected from the definition of δA. Also, increasing the perturbation amplitude the error in the output becomes worse.
It can be also noticed that adding axial planes, so having an overestimated system not only increases the stability of the matrix but also limits the propagation of inaccuracies into the system. For some combinations of number of planes and distances δA becomes minor than 1 and even if the perturbation of the azimuthal mode amplitudes is, for example, 100 Pa, the error in the radial mode amplitude is lower. Instead, in the case of small distances it can be seen that a perturbation of only few Pascal can induce an error of 100 Pa or more in the amplitude of the solution A_{mn}.
The same considerations can be made evaluating the error in the phase (instead of the amplitude) of the solution A_{mn} and also extended to the other propagating m modes, like in the case of δA and κ. An example considering the error in the phase of the solution

A_{mn} due to the perturbation in the amplitude of the azimuthal mode amplitude A_m is depicted in Fig.(5.6).

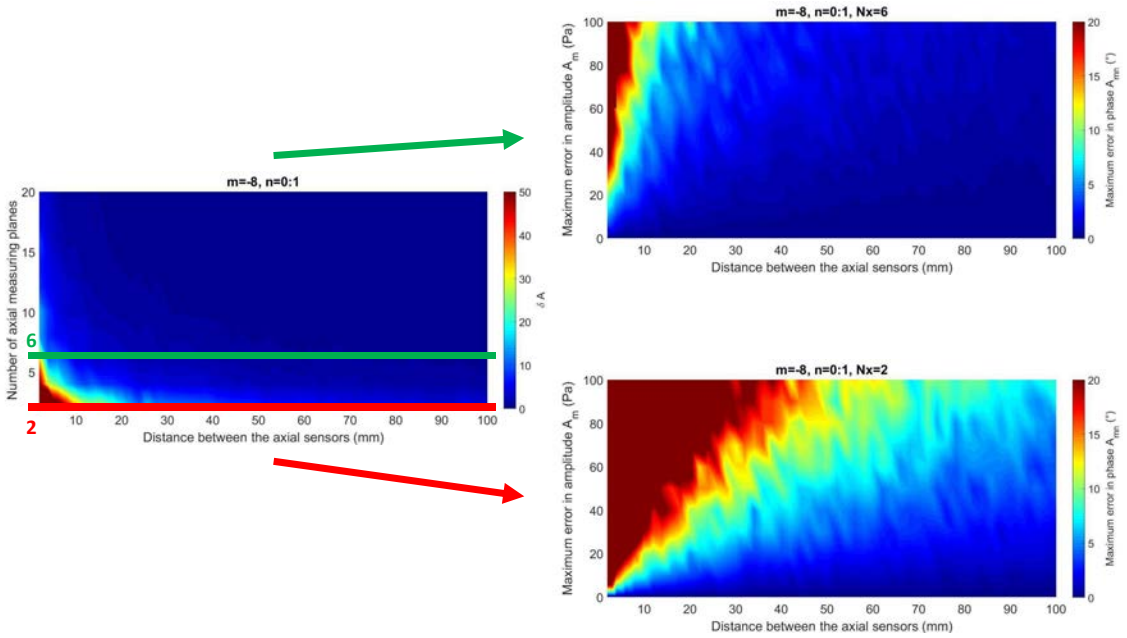

Figure 5.6.: Comparison of maximum errors in the phases of A_{mn} for $m = -8$ and $n = (0, 1)$ increasing N_x

5.2. Effects of non propagating modes

The analysis passes now to the azimuthal mode order $m = 32$, for which only the radial mode order $n = 0$ propagates whereas the others do not. The condition number and the relative error are compared at first respectively considering the first two and three radial mode orders.
It can be noticed that for the case with $n = (0, 1)$ the trend of δA and κ is similar to that of azimuthal mode order $m = -8$. Considering the change in scale, the values of these quantities are even smaller, and hence better, respect to those of $m = -8$ for the same number of axial planes and distance between them. The influence of the not propagating mode on the results is really small in this case because the mode decreases from its initial amplitude to the 0.01% of this initial value slowly along the x-axis, particularly in $\delta x = 9$ cm. However, from the plot of κ applying a change in scale it can be noticed that its value is higher with a small amount of sensors and small distances, like in case of $m = -8$, but also with more sensors and higher distances. This can be explained considering the presence of the exponential term $e^{ik_{mn}^{-}x}$ of the not propagating mode in the entries of

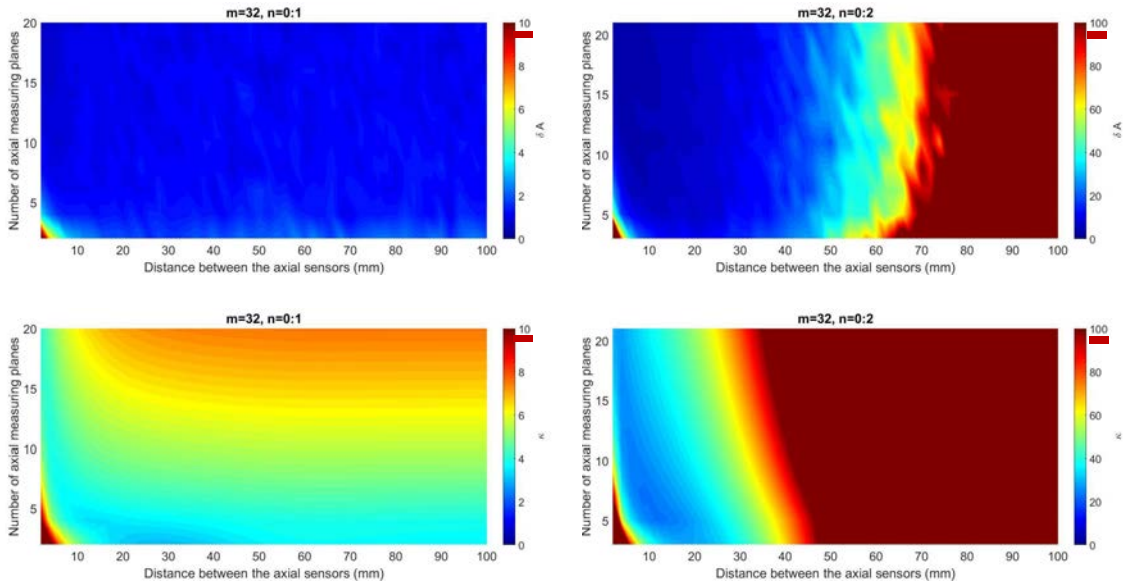

Figure 5.7.: Evolution of δA and κ for $m = 32$ adding radial modes into account

matrix $\mathbf{W}$, whose build up is shown in Eq.(2.22). Particularly, this term will be lower as the distance increases and so also the lowest eigenvalue ζ_{min} will decrease, causing an increase of the condition number κ.
Adding a radial mode into the analysis changes significantly the results, but the considerations made for the condition number κ are similar to the ones just explained. The not propagating mode with radial mode order $n = 2$ decreases faster from its initial amplitude to the 0.01% of it than the previous one with $n = 1$, particularly in $\delta x = 6\ cm$, because the absolute value of the imaginary component of k^{-}_{mn} is higher and so the exponential term $e^{ik^{-}_{mn}x}$ will decrease faster causing a higher condition number κ. This implies that increasing the distance between the axial measuring planes is not a good choice because it is more difficult to detect correctly the not propagating mode. Adding axial planes, the distance between them should be reduced in order to decrease the total distance between the first and the last plane and so avoid high condition numbers κ. All these considerations are also needed in order to explain the failure of optimization done with the full system in Eq.(2.19), explained more in details in subsection 4.2.1.
In Fig.(5.8) and (5.9) the plots above in the right side refer to the maximum error in amplitude of solution A_{mn} depending on the maximum perturbation in the amplitude of A_m whereas below in the right side the plots refer to the maximum error in phase of solution A_{mn}. The comparison is made increasing the number of axial planes and considering the case with the first three radial mode orders.

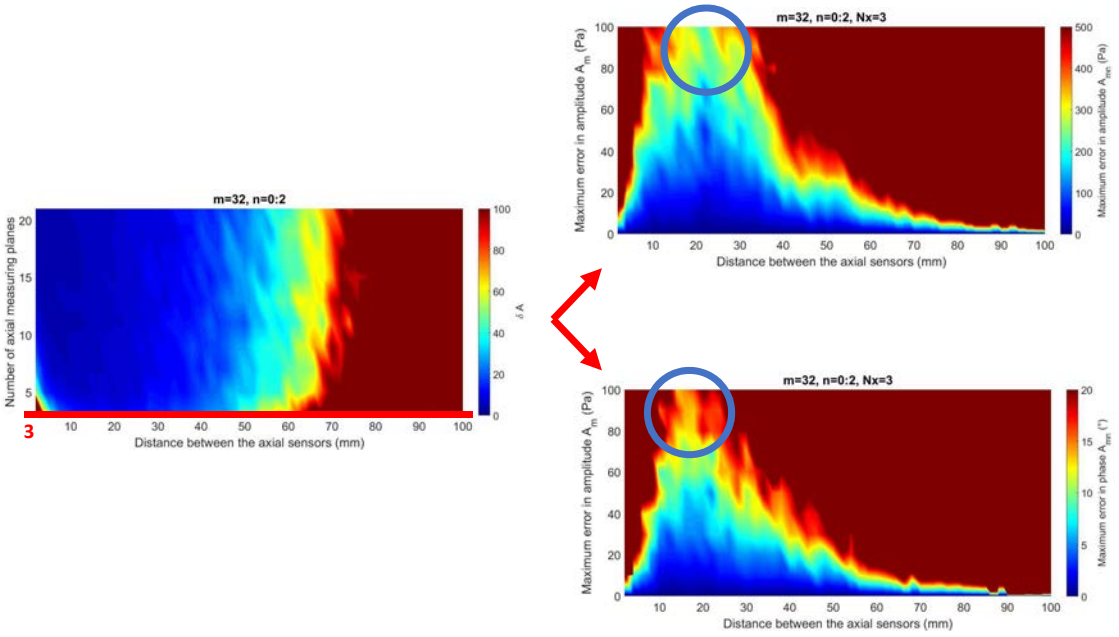

Figure 5.8.: Comparison of maximum errors of amplitude and phase for $m = 32$ and $n = (0, 1, 2)$ for $N_x = 3$

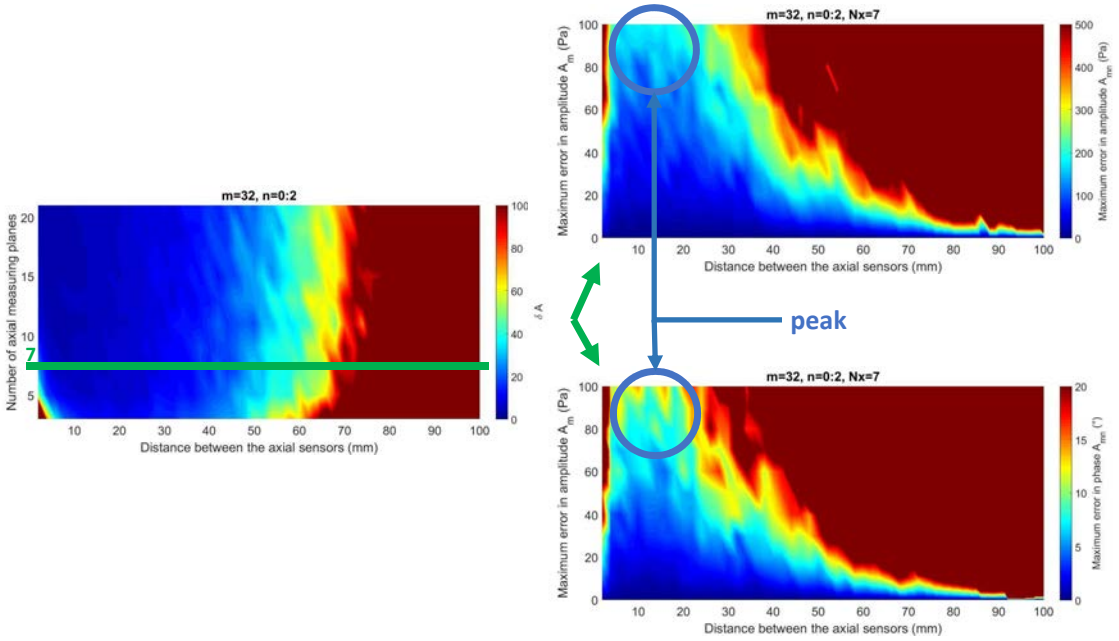

Figure 5.9.: Comparison of maximum errors of amplitude and phase for $m = 32$ and $n = (0, 1, 2)$ for $N_x = 7$

From the plots it can be noticed that an increase of N_x causes the decrease of the maximum error and alongside a shift to the left of the peak in which the propagation of the perturbation is lower. This trend is in line with those of δA and κ, whose values decrease as N_x increases and the distance decreases, like explained before.
Adding other radial modes to the analysis makes worse the search of optimization ranges of N_x and Δx in which the partition of the radial modes could be accurate because the condition numbers κ become really high due to the increasing of the absolute value of the imaginary part of k_{mn} in the exponential term in the entries of matrix $\mathbf{W}$ as the radial mode n increases.
Now the azimuthal mode order $m = -48$, which is not propagating for all the radial mode orders, is taken into account. The results and the considerations are similar to the previous case of $m = 32$ but with some differences due to the faster decay of the not propagating modes. Particularly, the mode with $n = 0$ decreases from its initial amplitude to the 0.01% of it in $\delta x = 5\ cm$ whereas the mode with $n = 1$ in $\delta x = 4\ cm$. The plots for δA and κ are reported below only for the first two radial mode orders and compared with the one of mode $m = 32$ for the first three radial mode orders in the right side. From

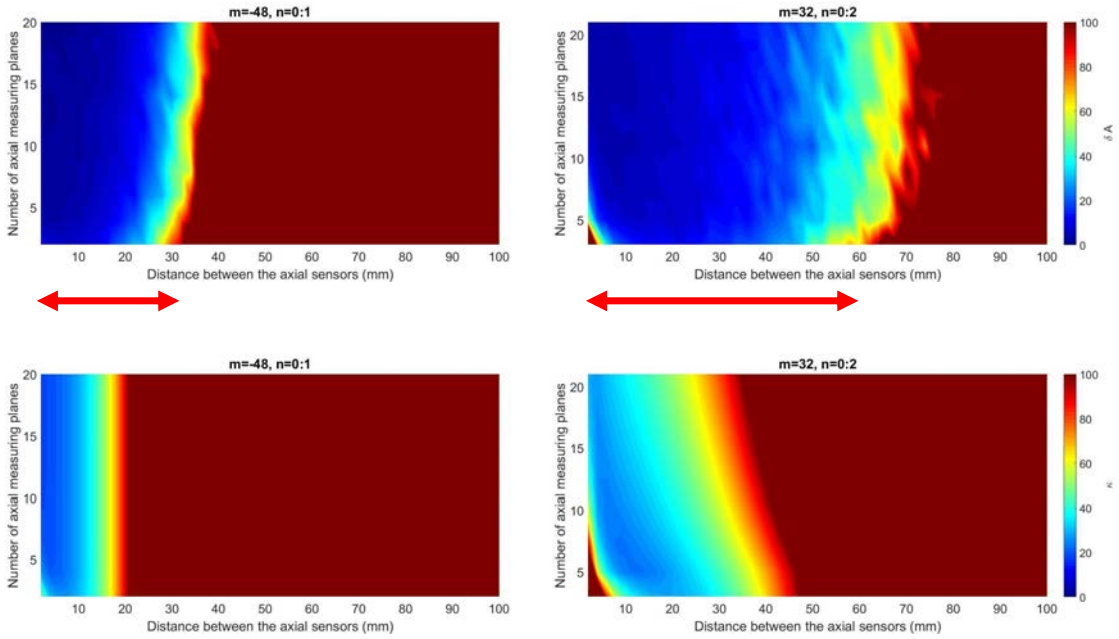

Figure 5.10.: Plots of δA and κ for $m = -48$ compared to those of $m = 32$

the comparison it can be noticed that the distances between the axial measuring planes should be even more decreased in order to minimize the values of the condition number and the relative error. Hence, the ranges in which the user can operate are increasingly smaller. In the plot below in the left side of Fig.(5.10) the condition number has similar values for every N_x depending on the distance. An explanation of this trend has been found observing the evolution of the matrix of eigenvalues $diag[\zeta_j]$ from Eq.(2.30) and it has been noticed that, in this case of only two radial mode orders, the two eigenvalues

first varies both and then, after a certain distance between the axial planes, equal for all the number of planes N_x, only the second becomes lower due always to the exponential term $e^{ik_{mn}^{-}x}$ for the radial mode order $n = 1$, that decreases faster than the one referred to the radial mode order $n = 0$.
If other radial mode orders are added to the system, an optimization is quite impossible to do because the good ranges are disappearing and the partition of the modes is successful only for a perturbation amplitude really close to zero and so requires a very strict measurement accuracy, otherwise the propagation of errors is very large and the system unstable. This can be noticed in Fig.(5.11) considering the evolution of Fig.(5.10) adding another radial mode order into account.

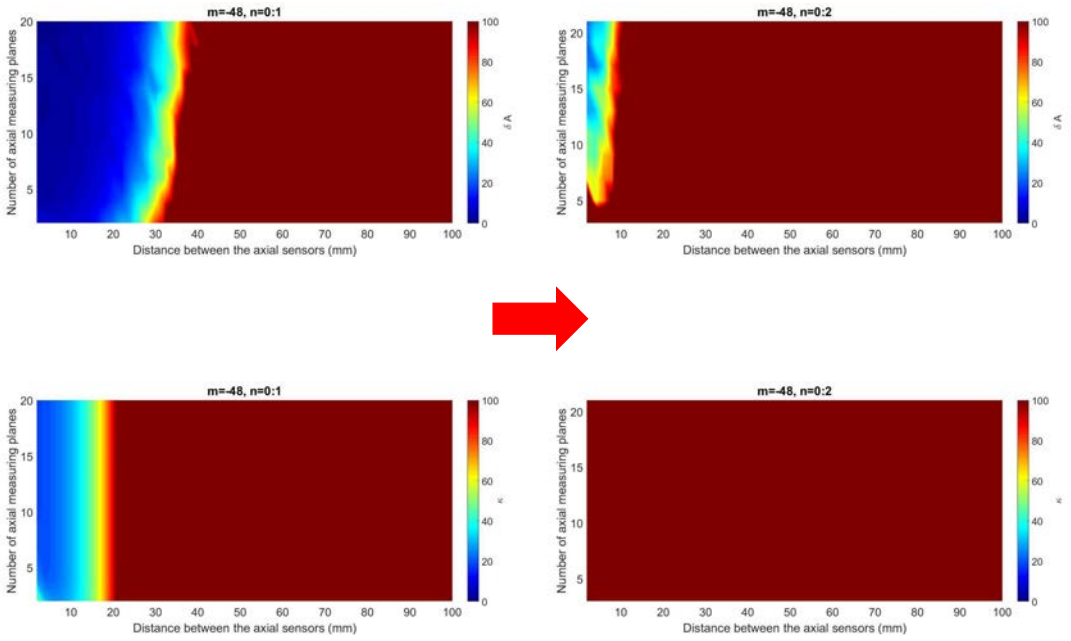

Figure 5.11.: Evolution of δA and κ for $m = -48$ adding a radial mode order into account

Considering other not propagating modes with a higher azimuthal mode order m, the values of δA and κ will be also higher (reaching an order of magnitude of 10^{15} or more) because of the increasing of the absolute value of the imaginary part of k_{mn}^{-}.

5.3. Effects of frequency

The results of the analysis done considering the second harmonic are now discussed and compared with those obtained considering the first harmonic. Always an input perturbation only in amplitude is added into the azimuthal mode amplitudes like in the first case

in Fig.(4.13). The reflected modes are also neglected.
The azimuthal mode orders that occur in this case vary from the previous case according to Eq.(2.2). Particularly, because of the increased frequency the number of propagating modes are more than before. This consideration can be derived from Eq.(2.14) of the axial wave number, noticing that the term under the square root increases as the product (kR), and hence the frequency, increases and so k_{mn} consists of only a real part for an higher amount of modes rather than before with a lower frequency. This consideration is seen below:

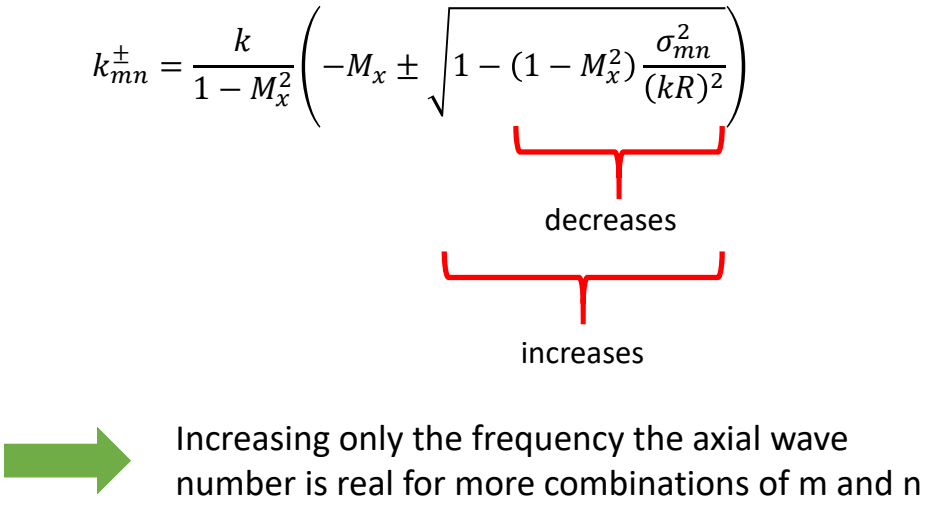

Figure 5.12.: Effect of increasing frequency on the axial wave number

The first azimuthal mode order considered is $m = 12$, for which all the considered radial mode orders are propagating. In the next figures the relative error δA and the condition number κ are plotted in the same manner of the previous plots and compared to that of the propagating mode $m = -8$ for the first harmonic in the right side.
Comparing $m = -8$ and $m = 12$ it can be noticed that the trends of δA and κ are similar for the first case in which two radial mode orders are considered whereas in the second case with all the considered radial modes are a bit different. Particularly in the case with $m = 12$ and $n = 0 : 4$, the bad-chosen positions (in red) come from an "expansion" of the case with $m = 12$ and $n = 0 : 1$, implying that more sensors and higher distances are better for an optimization and there are not alternate ranges of distance in which the values become higher or lower like in the case of $m = -8$. It can be supposed that maybe these alternate ranges occur at distances higher than $\Delta x = 100\ mm$, the last value of the analysis.

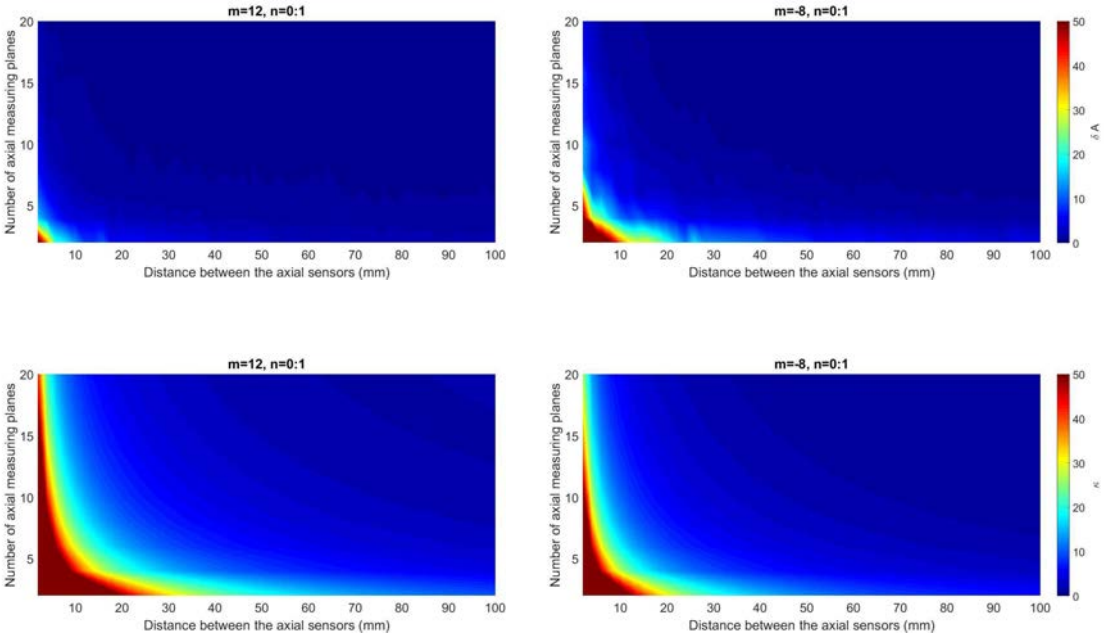

Figure 5.13.: Comparison of δA and κ for $m = 12$ and $n = (0, 1)$

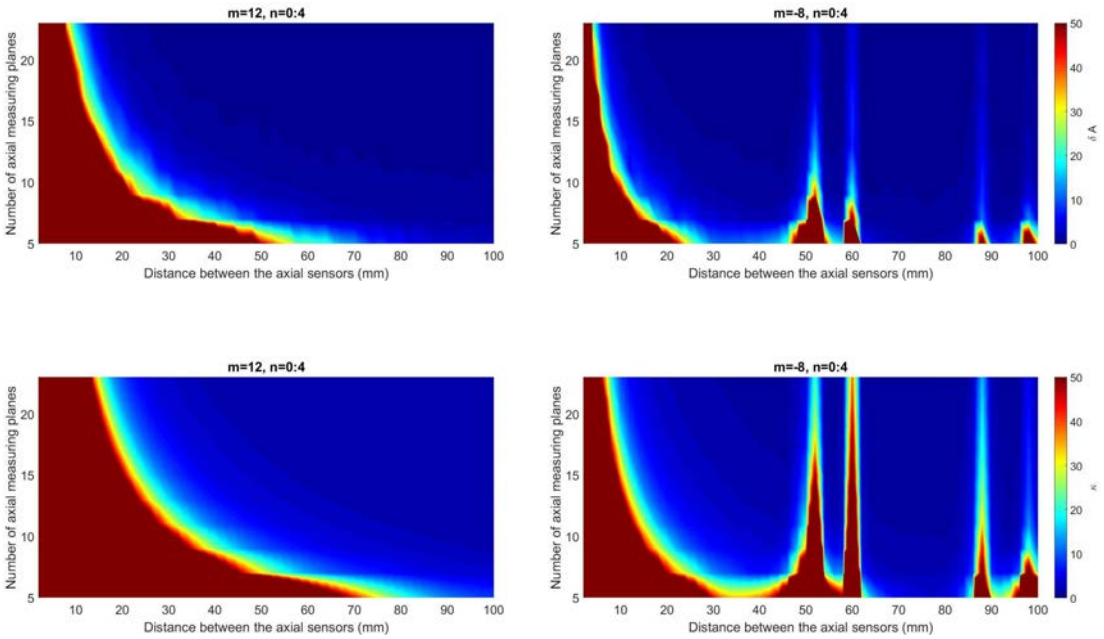

Figure 5.14.: Comparison of δA and κ for $m = 12$ and $n = (0, 1, 2, 3, 4)$

Also in this case of the second harmonic, the plots of the maximum errors reflect the trend of the relative error and the condition number for every number of axial planes. Increasing this number and also the distance between the measuring planes the propagation of the perturbations influences less the analysis and the results of solution A_{mn}.
The alternate ranges mentioned before however occur for higher azimuthal mode orders, like for example $m = -56$, for which δA, κ and the maximum errors in amplitude and phase of the solution are plotted below:

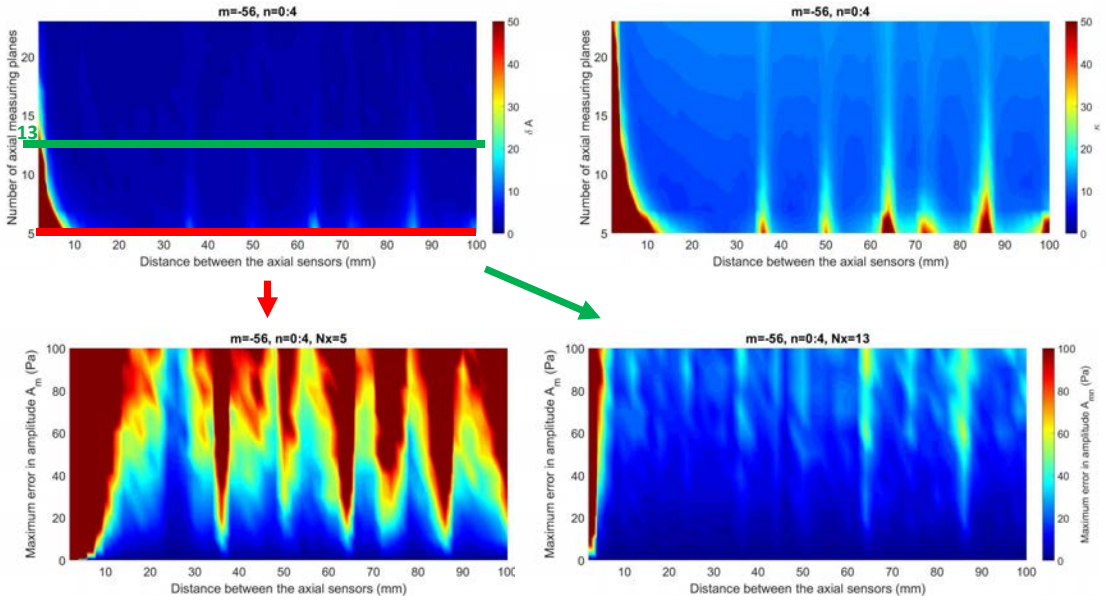

Figure 5.15.: Plot of δA, κ and the maximum errors in amplitude of A_{mn} for $m = -56$

In this case, in which all the radial mode orders are taken into account, only the last $n = 4$ is not propagating but, like $n = 1$ for $m = 32$ it does not influence so much the trend of δA and κ because it decreases very slow.
Finally for this case of the second harmonic, the results of the azimuthal mode order $m = 64$, which has the radial mode orders $n = (0, 1)$ propagating whereas the others $n = (2, 3, 4)$ not, are reported. For the first three modes the results are similar to those of all the other considered propagating azimuthal mode order m, but present some characteristics slightly different. Adding radial modes into the analysis, the trends of the relative error and the condition number approach to those of the azimuthal mode order $m = 32$.

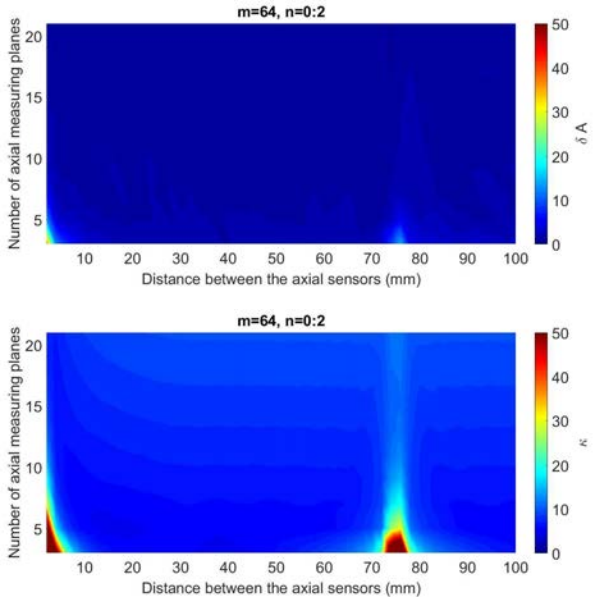

Figure 5.16.: Comparison of δA and κ for $m = 64$ an $n = (0, 1, 2)$

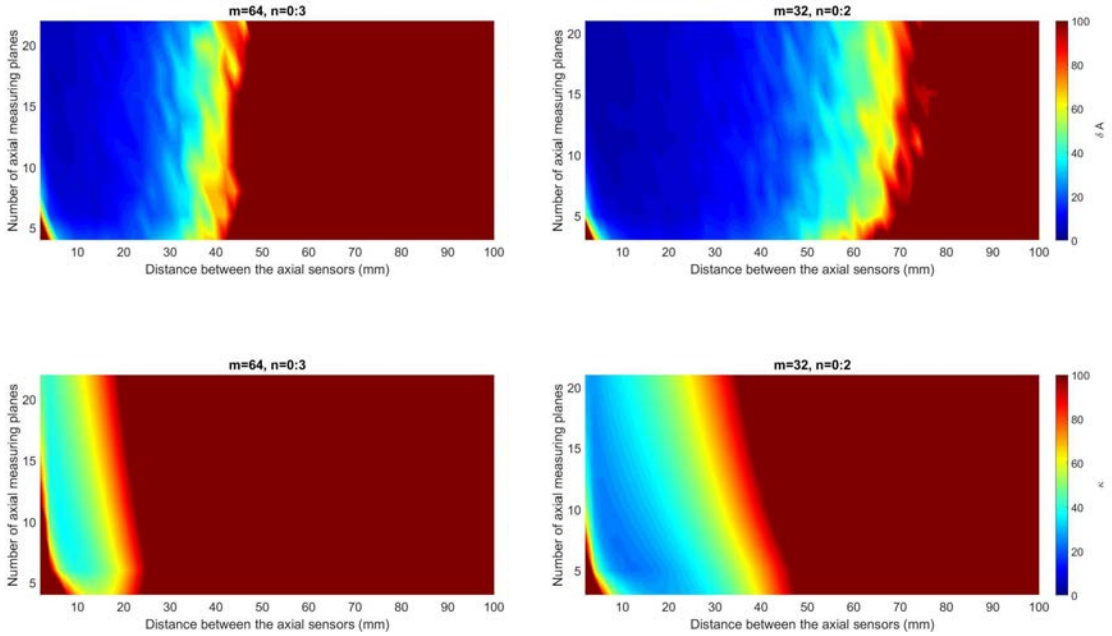

Figure 5.17.: Comparison of δA and κ for $m = 64$ an $n = (0, 1, 2, 3)$ with $m = 32$ and $n = (0, 1, 2)$

From Fig.(5.16) it can be noticed that for the first case with only the first three radial mode orders, the ranges in which δA and κ increase are located not only for small distances but principally around the distance $\Delta x = 75\ mm$. However, comparing these plots with the ones in Fig.(5.15) and Fig.(5.13) and (5.14), the values of δA and κ are correspondingly lower for the same number of axial planes and distance. Adding the radial mode order $n = 3$ into the analysis, it can be seen in Fig.(5.17) that the plots have the same trend of that for the azimuthal mode order $m = 32$ and radial mode orders $n = (0, 1, 2)$ plotted in the right side. Considering the plot of κ, the presence of the not propagating modes reduces for every number of axial planes the distance between them at which the solution can be detected quite correctly because the associated pressure decays really fast and the decreasing exponential term $e^{ik_{mn}x}$ causes the increase of the condition number κ and makes the system unstable. Also the propagation of inaccuracies is amplified.
The completely not propagating azimuthal mode orders, for example $m = -92$ and $m = -96$, present the same characteristics of the not propagating ones in the case of the first harmonic, like $m = -48$. The considerations are the same made before. Particularly, the mode amplitude decays from its initial value to the 0.01% of this value occur at least in $\delta x = 3\ cm$ for the first two radial mode orders.

5.4. Comparing effects of perturbations in amplitude and perturbations in phase

The comparison of how the different types of errors influence the results is now made. Particularly, it has been checked that the plots of the relative error δA are similar from those reported above varying the type of error whereas the plots of κ do not change.
However, it can be noticed by the following plots that a perturbation in phase, for example of 1°, added to the azimuthal mode amplitudes like in the second case of Fig.(4.13) has more influence than a perturbation in amplitude of 10 Pa. The accuracy in the measure of phase should so be more strict than that of amplitude. An example of this consideration can be found in Fig.(5.18) where in the left side for a number of axial planes the maximum error in the radial amplitudes chosen from all the repeated simulations of the same analysis is plotted. This maximum error depends on the maximum perturbation in phase added to the azimuthal mode amplitudes and on different distances between the axial planes.
From the comparison with the plots on the right side, in which only a perturbation in amplitude for the same modes is considered, it can be noticed that the maximum errors in the amplitude of the radial mode amplitudes A_{mn} are worse adding a perturbation in phase from 1° to 10° on A_m rather than adding a perturbation in amplitude from 10 to 100 Pa always on A_m. Like in all the previous cases, increasing the number of axial planes N_x is a solution to decrease the propagation of inaccuracies, like suggested from the two plots in the left side of Fig.(5.18), in which the only variable that is changing is N_x, particularly increasing from the plot above to the plot below.

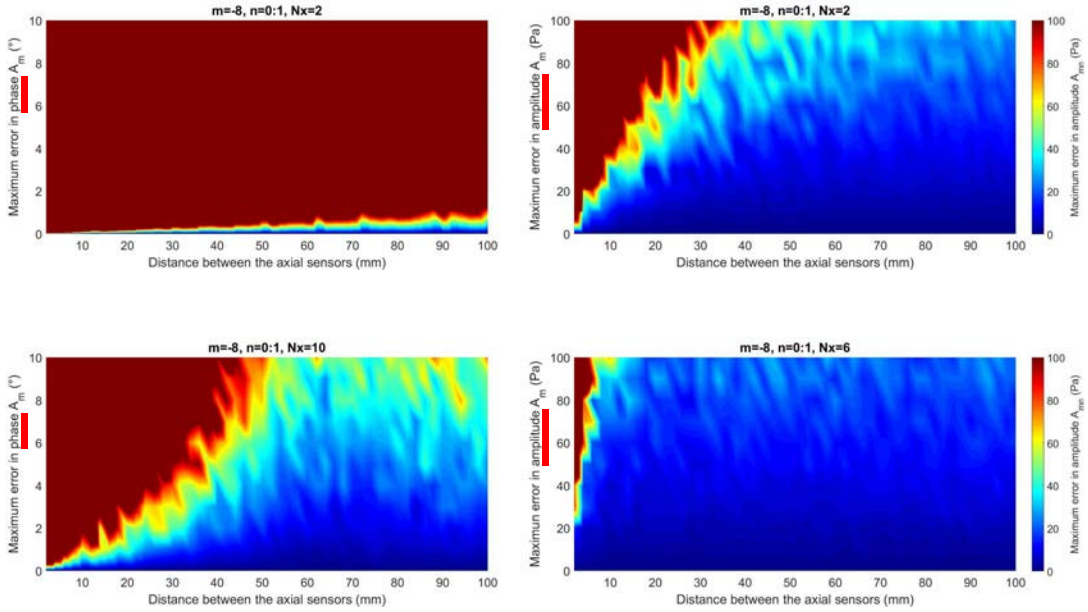

Figure 5.18.: Comparison of maximum errors for $m = -8$ with only a perturbation in phase on A_m

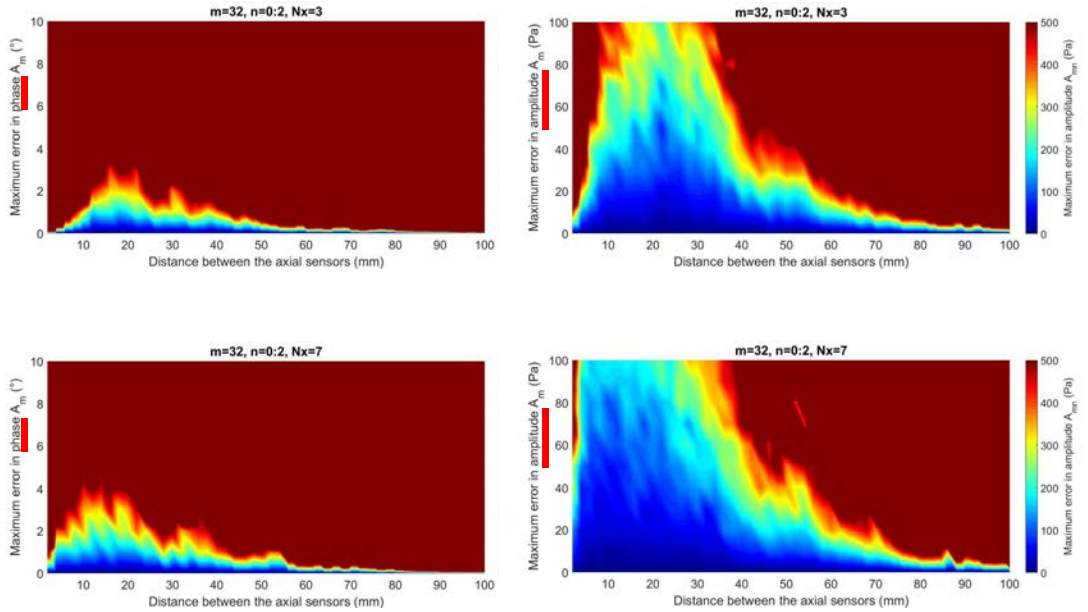

Figure 5.19.: Comparison of maximum errors in the amplitudes of the radial amplitudes for $m = 32$

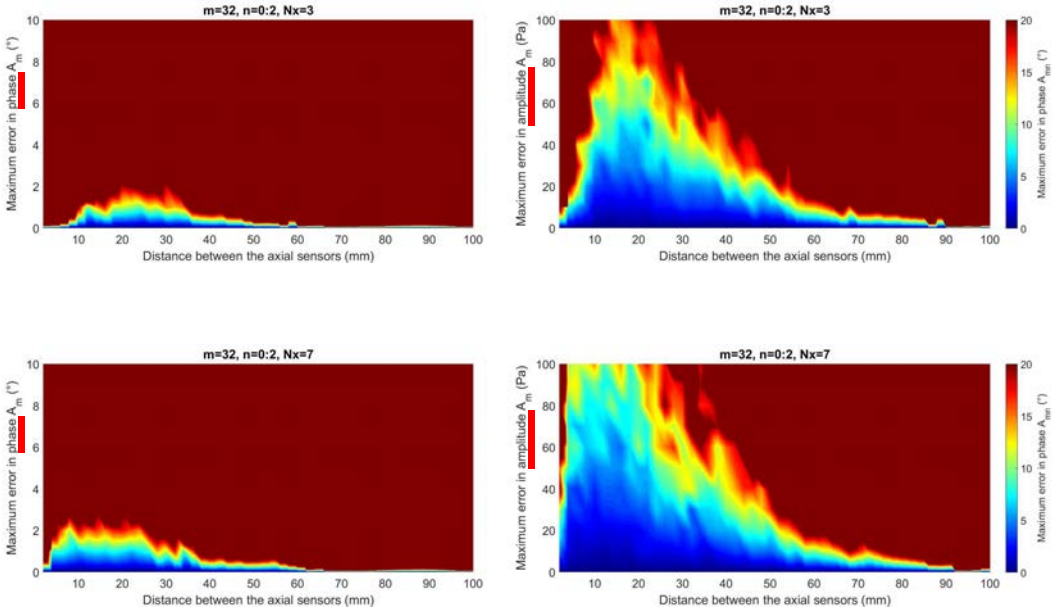

Figure 5.20.: Comparison of maximum errors in the phases of the radial amplitudes for $m = 32$

Another example is reported in Fig.(5.19) and Fig.(5.20) considering the azimuthal mode order $m = 32$, plotting the maximum errors in amplitude and phase of the solution A_{mn} for a different number of axial planes N_x and comparing them to the cases of only an amplitude perturbation. The change in scale has been done in order to see clearly in what range of distances the propagation of inaccuracies were minimized.
Also in this case, an increase of number of axial planes induces the decrease of the maximum error and the peak in which the propagation of the perturbation is lower shifts to the left, where the distances between the axial planes are smaller.
Finally, adding a perturbation in both amplitude and phase in the azimuthal mode amplitudes, like the third case in Fig.(4.13), generates similar results as before, amplifying the maximum errors because even the perturbations are higher.

5.5. Effects of reflected propagating modes

As the last comparison, also the reflected propagating modes are taken into account. The case of azimuthal mode order $m = -8$ and the first two radial mode orders $n = (0, 1)$ which are both propagating is shown. The plots of the relative error and the condition number have a different trend from the one of the case without the reflected modes, plotted in the right side of Fig.(5.21).
Like it can be seen from the left side of Fig.(5.21), the optimization of the measuring array

considering also the reflected modes is more difficult to implement because the ranges in which δA and κ become higher increases compared to the previous case. Particularly, for a small number of sensors the ranges of distance in which δA and κ are minimized alternates along the x-axis. For example, the optimization for the minimum number of measuring planes $N_x = N_n = 4$ can be done in the ranges of distances $\Delta x = 22 - 30\ mm$, $\Delta x = 38 - 48\ mm$, $\Delta x = 56 - 64\ mm$, $\Delta x = 72 - 82\ mm$ and $\Delta x = 88 - 100\ mm$. For $N_x >> N_n$ all the distances between the axial planes can be taken into account for an optimization.
An explanation for this trend could be the expansion of matrix $\mathbf{W}$, which size is in this case doubled because the number of considered modes and also the required minimum number of axial planes in order to detect the modes amplitudes are doubled. This seems to bring to a worse condition of the matrix.

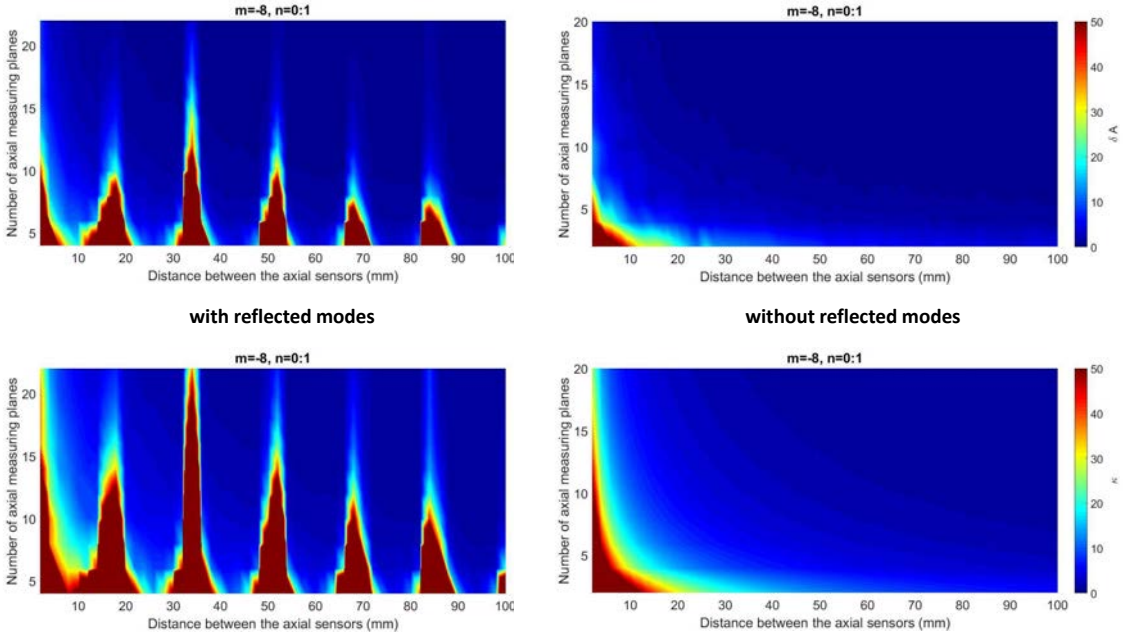

Figure 5.21.: Plot of δA and κ for $m = 8$ considering the reflected propagating modes

The same considerations can be made taking into account a propagating mode in the case of the second harmonic, like the azimuthal mode order $m = 12$ with radial mode orders $n = (0, 1)$. In this case, the optimization is even harder to do compared to the previous case of $m = -8$ because the ranges in which δA and κ become higher are duplicated, as highlighted in Fig.(5.22).

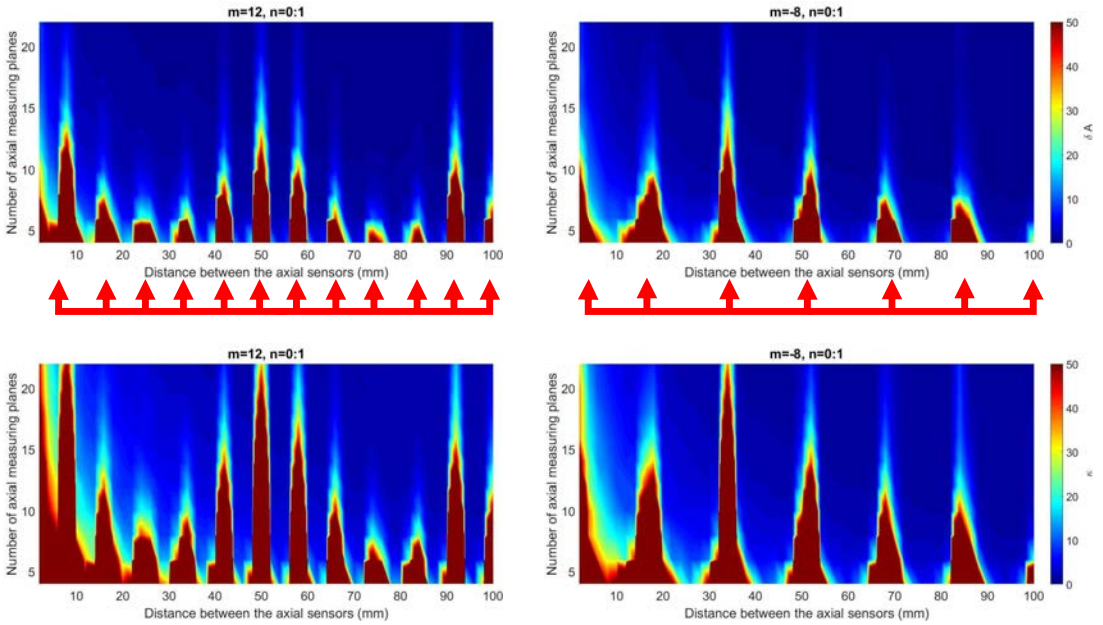

Figure 5.22.: Plot of δA and κ for $m = 12$ considering the reflected propagating modes

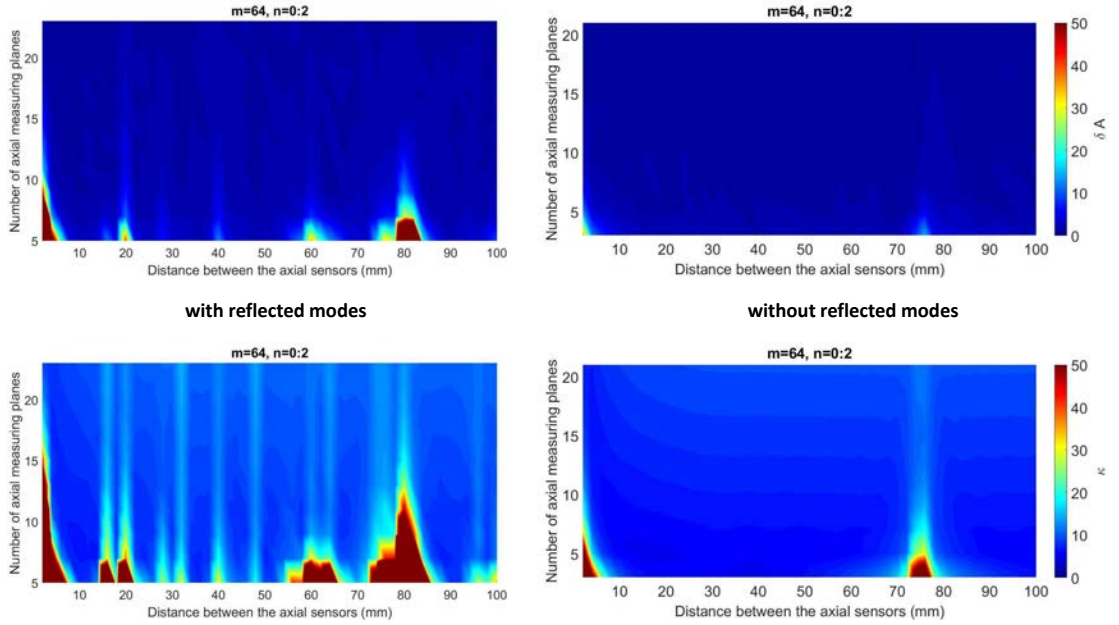

Figure 5.23.: Plot of δA and κ for $m = 64$ and $n = (0, 1, 2)$ considering the reflected propagating modes

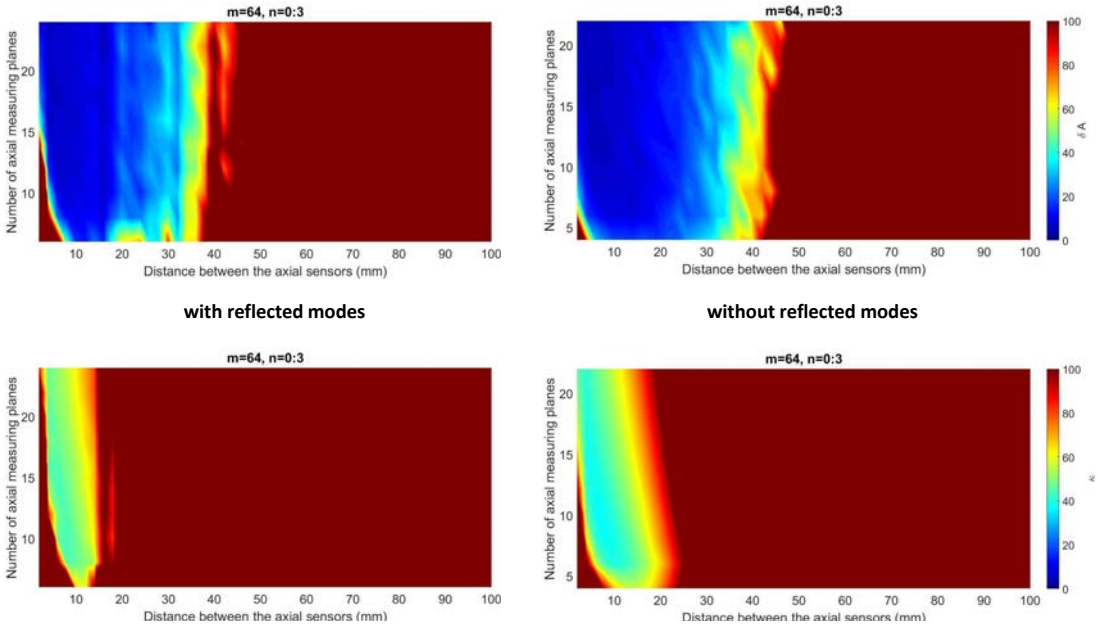

Figure 5.24.: Plot of δA and κ for $m = 64$ and $n = (0, 1, 2, 3)$ considering the reflected propagating modes

In the last Fig.(5.23) and (5.24), the results for the azimuthal mode order $m = 64$, for which the radial mode orders $n = (0, 1)$ propagate whereas the others $n = (2, 3, 4)$ do not, is reported. In the case with n from 0 to 3, the not propagating mode influences badly the trend of the relative error and the condition number as in the case where the reflecting modes are not present, plotted in the right side. The same considerations done in section 5.2 regarding the presence of the decreasing exponential term $e^{ik_{mn}^{-}x}$ and its consequences can be used to explained this trend, for which high distances between the axial planes are not to choose for an optimization.

5.6. Conclusions

From all the presented results the following conclusions can be drawn:

- increasing the number of radial mode orders n taken into account the trends of κ and δA get worse for every azimuthal mode order m. Particularly for propagating modes, if increasing distances between the axial planes is a good choice for all the number of axial planes when considering the first two or three or also four radial mode orders, this is not more true adding other radial propagating modes into account and the distances for which the values of δA and κ stay low changes alternately according to the number of axial planes;

- the not propagating modes have requirements for the optimization that are opposite in order to detect correctly the radial amplitudes. They influences negatively the condition of matrix **W** due to the exponential term $e^{ik_{mn}^{-}x}$ and the imaginary part of k_{mn}^{-} which absolute value increases as the azimuthal mode order m and the radial mode order n increase. This induces a faster decreasing of the pressure amplitude associated to the mode along the duct. Hence, for the optimization, increasing the distance between the axial planes is to avoid and adding axial planes the distance has to be further reduce in order to decrease the total distance between the first and the last measuring plane. A distance that could fit in order to detect both propagating and non propagating has to be found;

- considering the second harmonic and hence the frequency, the number of propagating modes increases so the analysis can be carried out successfully for more modes. The differences between the effects of the propagation or not propagation of the modes are the same as in the case of the first harmonic;

- an error in phase, for example, of 1° on the azimuthal mode amplitudes A_m propagates more intensively on the system than an error in amplitude of 10 Pa, causing an higher error on the radial mode amplitudes A_{mn}. Therefore, the measurements on the phase of the azimuthal mode amplitudes should be more strict than the ones on the amplitudes in order to limit the propagation of inaccuracies;

- considering also the reflected propagating modes into account, the ranges for optimization become smaller and the distances for which δA and κ stay low changes according to the number of axial planes. Considering the first two radial mode orders, only for $N_x >> N_n$, almost all the distances are good.

From all these considerations and figures it is important to notice that an optimization in order to detect all the considered modes presents many difficulties. Every mode has a different range of distances that permits the right detection and partition of the radial modes, so an optimization valid for all the modes is hard to implement and requires accuracy and time. However, it is seen that having a number of planes really higher than the required minimum and small distances in order to not extend the array too much is generally the best choice for the optimization of a measuring grid that tries to decompose all the modes. Particularly, looking on all the results, it can be recommended that a distance of $\Delta x = 10$ mm between the axial planes could be an initial value for further improvements on the optimization. This distance is associated to a good analysis quality for almost all the considered number of axial planes and the expected modes.

6. Summary

The purpose of this work was to carry out a radial mode analysis in order to investigate the sound field of a multi-stage axial compressor test rig, starting from acoustic pressure measurements. Because the quality of the analysis is influenced by the arrangement of the measuring grid, an optimization about the number of sensors and the distance between them is required in order to decompose experimentally the field with accuracy.
A theoretical model based on a solution of the wave equation considering some assumptions on the flow characteristics is used.
The first encountered issue was to calculate the eigenvalues σ_{mn} and Q_{mn} of the radial distribution for every mode of azimuthal order m and radial order n. The problem was that the analytical solver needs an initial guess near of the solution in order to find it, but this guess changes for every combination of (m, n). The initial guess is found adding a constant to the previously solution $\sigma_{m(n-1)}$. Then a check is made looking if the solution is correct or not. If not, the initial guess is varied by other constants and the resulting new solution is checked again. With this method all the eigenvalues of the considered combinations of m and n have been found.
The pressure is then calculated along the duct as a superposition of some dominant acoustic modes, previously determined experimentally. The measuring grid consists of sensors mounted flush with the duct wall. Arrangements of equally and also randomly spaced sensors in the azimuthal direction have been tried.
From these values of pressure a radial mode analysis in order to separate the mode amplitudes is implemented. Also a perturbation on the pressure values has been added into the system and its propagation has been investigated in order to evaluate the accuracy with which the pressure has to be measured.
The principal issue coming from these analysis originated from the fast decay of the not propagating modes. These have an imaginary component of axial wave number that, due the exponential term $e^{ik^{\pm}_{mn}x}$ that defines the axial pressure distribution, causes an instability of system even higher as m, n and the distance x increase. Also the big size of the matrix and the presence of similar columns for $-m$ and m could influences negatively the condition of the matrix. A mode decomposition and an optimization was really hard to do in reasonable time.
Another way to make a radial mode analysis is to split the total system into two parts, one referring to the azimuthal mode analysis and one to the properly radial one. Particularly, this has to be made for every azimuthal mode order m that results from a supposed already completed azimuthal mode analysis. This implies that an optimization of the measuring grid only in the axial direction has to be carried out.
Some reasonable assumptions has been made in order to simplify the analysis:

- only the modes predicted from Tyler and Sofrin by Eq.(2.2) and coming from the

rotor-alone mechanism and the interaction of the first rotor with the IGV and with the first stator are considered;

- the radial mode amplitudes have for every mode the same amplitude but random phase;

- first all the reflected modes and then only the not propagating ones coming from the inlet are neglected.

Particularly, this last assumption can be explained considering that the not propagating modes decrease really fast from the IGV to the inlet so, when they are to be reflected their amplitude and the associated pressure can be neglected.
In order to assess the analysis quality the condition number of the system matrix and the relative error of radial mode amplitudes coming from multiple iterations are studied. Particularly, the accuracy of the results is higher as the values of κ and δA are lower. Also the maximum errors in amplitude and phase of the solutions are studied according to a perturbation added gradually to the system.
The optimization of the measuring grid has to be done exactly looking for which combination of number of axial planes and distance between them the values of the condition number and the relative error are kept low. From an analysis of the results, it comes out that every (m, n)-mode has a different range of combinations in which the analysis quality can be considered good.
Particularly, considering completely propagating modes, it is seen that increasing the number of axial planes and the distance between them is the best choice to implement in order to maximize the accuracy and minimize the propagation of noise errors through the system. Adding more radial mode orders into account, the number of axial planes for which this consideration remains true has to be really higher than the required minimum number of axial planes, determined from the Nyquist theorem.
Instead, when some radial mode orders of the considered azimuthal order m are not propagating high distances between the sensors are to avoid because of the fast decreasing along the duct, that produce high condition number due to the extremely small value assumed by $e^{ik_{mn}x}$. This value decreases as the distance increases and as the absolute value of the imaginary component of k_{mn} increases when the azimuthal mode order m and the radial mode order n increase. Particularly, the radial amplitudes coming from the analysis are really higher than the original ones.
Another conclusion obtained from the analysis of the results is that the measurements on the phase of the azimuthal mode amplitudes require more accuracy than the measurements on the amplitude because a perturbation in phase propagates more negatively on the results than a perturbation in amplitude.
Carrying out an analysis without perturbations, the radial mode amplitudes are well detected for all the modes.
Looking for the next steps, an optimization in order to find some values of the parameters grid that can be used for an experimental radial mode analysis can be carried out. This optimization will look into the good ranges found in this study of the grid parameters for which the accuracy of the solution is better. Every single expected mode m has to be studied separately. However, in a first look on the results a distance of $\Delta x = 10\ mm$ could be a starting point for an optimization in order to find correctly most of the radial

amplitudes of the selected modes. Also the geometrical characteristics of the compressor have to be taken into account in order to study the possibility of building up a measuring array with this distance. Because the ducted section at the inlet before the IGV is not so long, maybe the analysis could be done at the outlet.
In addition, an analysis taking into account more azimuthal mode orders m and radial mode orders n can be implemented. Also a way in order to study the effect of the reflected non propagating mode can be searched.
This analysis does not give directly the impact on force response but it is needed in a second step for improving and validating the predictions done by a CFD solver.

Bibliography

[1] Behn, M. ; Kisler, R. ; Tapken, U.: Efficient Azimuthal Mode Analysis using Compressed Sensing. In: *Proceedings of the 22th AIAA/CEAS Aereoacustics Conference*, 2016

[2] Bolleter, U. ; M.J.Crocker: Theory and Measurements of Modal Spectral in Hard-Walled Cylindrical Ducts. In: *Journal of Acoustical Society of America* 51 (1972), pp. 1439–1447

[3] Enghardt, L. ; Tapken, U. ; Kornow, O. ; Kennepohl, F.: Acoustic Mode Decomposition of Compressor Noise under the Consideration of Radial Flow Profiles. In: *Proceedings of the 11th AIAA/CEAS Aereoacustics Conference*, 2005

[4] Enghardt, L. ; Zhang, Y. ; Neise, W.: Experimental Verification of a Radial Mode Analysis Technique Using Wall-Flush Mounted Sensors. In: *Journal of Acoustical Society of America* (1999)

[5] Heidelberg, L. ; Hall, D.G.: Inlet Acoustic Mode Measurements in the Inlet of a Turbofan Engine. In: *AIAA Journal of Aircraft* 32 (1996), No. 4

[6] Joppa, P.D.: Acoustic Mode Measurements in the Inlet of a Turbofan Engine. In: *AIAA Journal of Aircraft* 24 (1987), No. 9

[7] Moore, C.J.: In-Duct Investigation of Subsonic Fan "Rotor Alone" Noise. In: *Journal of Acoustical Society of America* 51 (1972)

[8] Rademaker, E.R. ; Sijtsma, P. ; Tester, B.J.: Mode Detection with an Optimised Array in a Model Turbofan Engine Intake at Varying Shaft Speeds. In: *Proceedings of the 7th AIAA/CEAS Aeroacustics Conference*, 2001

[9] Tapken, U.: *Analyse und Synthese akustischer Interaktionsmoden von Turbomaschinen*, Technische Universität Berlin, Ph.D. Thesis, 2015

[10] Tapken, U. ; Enghardt, L.: Optimization of Sensor Arrays for Radial Mode Analysis in Flow Ducts. In: *Proceedings of the 12th AIAA/CEAS Aereoacustics Conference*, 2006

[11] Terstegen, M. ; Sanders, C. ; Jeschke, P. ; Schoenenborn, H.: Rotor-Stator Interactions in a 2.5-Stage Axial Compressor, Part I: Experimental Analysis of Tyler-Sofrin Modes. In: *Proceedings of the 15th International Symposium on Unsteady Aeroacoustics and Aeroelasticity of Turbomachines*, 2018

[12] Tyler, J.M. ; Sofrin, T.G.: Axial Flow Compressor Noise Studies. In: *SAE Transaction* Vol. 70. 1962, pp. 309–332

A. Description of the split system into an azimuthal and a radial mode analysis

The steps contained in this Appendix are made following [9]. As described in subsection (2.3.1), supposing that an azimuthal mode analysis has been already carried out, for every m mode the following system can be solved in order to find the radial mode amplitudes:

$$\mathbf{A_m} = \mathbf{W_m} \cdot \mathbf{a}. \tag{A.1}$$

where $\mathbf{A_m}$ is the vector of the measured azimuthal mode amplitudes of order m, $\mathbf{a}$ the vector of radial mode amplitudes and $\mathbf{W_m}$ the matrix with all the other factors in Eq.(2.26). The vector of the amplitudes of modes with azimuthal mode order m and radial mode order n is defined as [9]:

$$\mathbf{a} = (A_{m,0}, A_{m,1}, ..., A_{m,N})^t \tag{A.2}$$

where the subscripts refer to the order of modes as follows:

- azimuthal mode order m;
- radial mode order: $0, 1, ..., N \sim (0,+), (0,-), ..., (max(n),-)$.

Hence, the dimension of vector $\mathbf{a}$ corresponds to the number of modes considered in (+) and against (-) the flow direction. The vector of the measured azimuthal mode amplitudes of order m is defined as follows [9]:

$$\mathbf{A_m} = (A_m(x_1, r_1,), A_m(x_1, r_2), ..., A_m(x_{N_x}, r_{N_r}))^t \tag{A.3}$$

where its dimension is $(N_x N_r \times 1)$. The matrix $\mathbf{W_m}$ is built up as follows [9]:

$$\mathbf{W_m} = \begin{pmatrix} \Psi_{m,0}(x_1, r_1) & \Psi_{m,1}(x_1, r_1) & ... & \Psi_{m,N}(x_1, r_1) \\ \Psi_{m,0}(x_1, r_1) & \Psi_{m,1}(x_1, r_1) & ... & \Psi_{m,N}(x_1, r_1) \\ . & . & . & \\ . & . & . & \\ . & . & . & \\ \Psi_{m,0}(x_{N_x}, r_{N_r}) & \Psi_{m,1}(x_{N_x}, r_{N_r}) & ... & \Psi_{m,N}(x_{N_x}, r_{N_r}) \end{pmatrix}. \tag{A.4}$$

Its dimension is, hence, $(N_x N_r \times 2N_n(m))$. The axial and radial eigenfunctions are contained in [9]:

$$\Psi_{m,n}(x_j, r_k) = e^{ik_{mn}^{\pm} x} f_{mn}(r_k). \tag{A.5}$$

Between the vector of complex pressure $\mathbf{p}$ in Eq.(2.19) and the vector of the azimuthal mode amplitudes $\mathbf{A_m}$ the following relation is valid [9]:

$$\mathbf{p} = \sum_{m=0}^{M} \mathbf{V_m} \cdot \mathbf{A_m} \tag{A.6}$$

where the matrix $\mathbf{V_m}$ is built up like follows:

$$\mathbf{V_m} = \begin{pmatrix} e^{im\Phi_1} & 0 & ... & 0 \\ e^{im\Phi_2} & 0 & ... & . \\ . & . & ... & . \\ . & . & ... & . \\ . & . & ... & . \\ e^{im\Phi_{N_\Phi}} & 0 & ... & . \\ 0 & e^{im\Phi_1} & ... & . \\ . & . & ... & . \\ . & . & ... & . \\ . & . & ... & . \\ . & e^{im\Phi_{N_\Phi}} & ... & . \\ . & 0 & ... & e^{im\Phi_1} \\ . & . & ... & . \\ . & . & ... & . \\ . & . & ... & . \\ 0 & 0 & ... & e^{im\Phi_{N_\Phi}} \end{pmatrix}. \tag{A.7}$$

Hence, combining Eq.(A.1) with Eq.(A.6) it follows that [9]:

$$\mathbf{p} = \sum_{m=0}^{M} \mathbf{V_m} \cdot \mathbf{W_m} \cdot \mathbf{a}. \tag{A.8}$$

B. Calculation of the eigenvalues

The steps contained in this Appendix are made following [9]. The calculation of the eigenvalues is based on the resolution of the differential equations that define the hard-walled acoustic boundary conditions, as explained in subsection (4.1.1). The equations are here reported:

$$r = R_i : J'_m(\eta\sigma_{mn}) + Q_{mn}Y'_m(\eta\sigma_{mn}) = 0 \tag{B.1}$$

$$r = R : J'_m(\sigma_{mn}) + Q_{mn}Y'_m(\sigma_{mn}) = 0. \tag{B.2}$$

After some manipulation the following relations can be derived [9]:

$$J'_m(\eta\sigma_{mn})Y'_m(\sigma_{mn}) - J'_m(\sigma_{mn})Y'_m(\eta\sigma_{mn}) = 0, \tag{B.3}$$

$$Q_{mn} = -\frac{J'_m(\sigma_{mn})}{Y'_m(\sigma_{mn})}. \tag{B.4}$$

Using the following identities the eigenvalues can be computed directly from the Bessel functions [9]:

$$2J'_m(x) = J_{m-1}(x) - J_{m+1}(x), \tag{B.5}$$

$$J'_0(x) = -J_1(x), \tag{B.6}$$

$$2Y'_m(x) = Y_{m-1}(x) - Y_{m+1}(x), \tag{B.7}$$

$$Y'_0(x) = -Y_1(x). \tag{B.8}$$

It then follows for $m = 0$:

$$J_1(\eta\sigma_{mn})Y_1(\sigma_{mn}) - J_1(\sigma_{mn})Y_1(\eta\sigma_{mn}) = 0, \tag{B.9}$$

$$Q_{mn} = -\frac{J_1(\sigma_{mn})}{Y_1(\sigma_{mn})} \tag{B.10}$$

and for $m > 0$:

$$\begin{aligned}&(J_{m-1}(\eta\sigma_{mn}) - J_{m+1}(\eta\sigma_{mn}))(Y_{m-1}(\sigma_{mn}) - Y_{m+1}(\sigma_{mn}))\\ &- (J_{m-1}(\sigma_{mn}) - J_{m+1}(\sigma_{mn}))(Y_{m-1}(\eta\sigma_{mn}) - Y_{m+1}(\eta\sigma_{mn})) = 0,\end{aligned} \tag{B.11}$$

$$Q_{mn} = \frac{J_{m+1}(\sigma_{mn}) - J_{m-1}(\sigma_{mn})}{Y_{m-1}(\sigma_{mn}) - Y_{m+1}(\sigma_{mn})} \tag{B.12}$$

like reported in subsection (4.1.1).